Journal Title
XX(X):1–24

DOI: 10.1177/ToBeAssigned
www.sagepub.com/
SAGE

Force-Amplifying N-Robot Transport System (Force-ANTS) for Cooperative Planar Manipulation without Communication

Zijian Wang[1,2] and Mac Schwager[1]

Abstract

We propose the concept of a Force-Amplifying N-Robot Transport System (Force-ANTS) to coordinate the manipulation forces from a group of robots in order to transport a heavy object in a planar environment. Our approach requires no explicit communication among robots. Instead, we prove that robots can use local measurements of the object's motion at their attachment points as implicit information for force coordination. A leader (either a robot or human) can guide the whole group towards the destination by applying a relatively small force, whose effect is amplified by the follower robots as they align their forces with the leader's. Two Force-ANTS implementations are introduced and analyzed, accounting for two different classes of object dynamics: small objects where kinetic friction dominates, and large objects where inertia and viscous friction dominate. Our approach can be used as a modular system for transporting heavy objects of various sizes in many real-life applications. Simulations with up to 1000 robots and experiments using four custom-built robots are conducted to validate our approach. We also conduct human-robot cooperation experiments where the human force is amplified by three follower robots.

Keywords

Multi-Robot Manipulation, Object Transport by Swarm Robots, Human-Robot Cooperative Manipulation

1. Introduction

In this paper, we propose an algorithm for a group of robots to cooperatively move an object that is too heavy for an individual robot to move alone. We introduce a control and coordination architecture called Force-Amplifying N-Robot Transport System (Force-ANTS) that achieves force coordination among a group of robots without any explicit communication network. The robots instead use sensors that measure the motion of the object itself to coordinate their actions. The algorithm is simple and practical, as shown in our hardware experiments, and it is provably scalable and convergent, as addressed in our analysis. In the Force-ANTS, a leader (either a robot or a human) is the only one who knows the desired trajectory. The leader steers the group towards the destination by adjusting its own force, while the follower robots reinforce the leader's intention by aligning their forces with the leader's. An overview of our approach is shown in Figure 1.

The highlight of our approach is that no communication is needed among all the robots, leading to a scalable and easily configurable solution. Communication is a key bottleneck in coordination algorithms used in many multi-robot systems, for example, Zhang and Tian (2010), Li and Zhang (2010). Communication networks tend to be noisy, time-delayed, limited by bandwidth, power hungry, and they introduce complexity in routing algorithms and hardware. By eliminating the need for communication, our approach can achieve the coordination of hundreds or thousands of robots. Moreover, since every robot operates in a "standalone" mode, adding/removing robots to the system can be as simple as attaching or detaching the robots to or from the object, without the difficulty of updating the communication protocol or re-configuring software. The robots achieve force coordination without communication by measuring the motion of the object at their attachment points on the object. This information is accessible locally by all the robots if equipped with appropriate sensors.

[1]Department of Aeronautics and Astronautics, Stanford University, Stanford, CA, USA
[2]Department of Mechanical Engineering, Boston University, Boston, MA, USA

Corresponding author:
Zijian Wang, Department of Aeronautics and Astronautics, Stanford University, Stanford, CA 94305, USA
Email: zjwang@stanford.edu

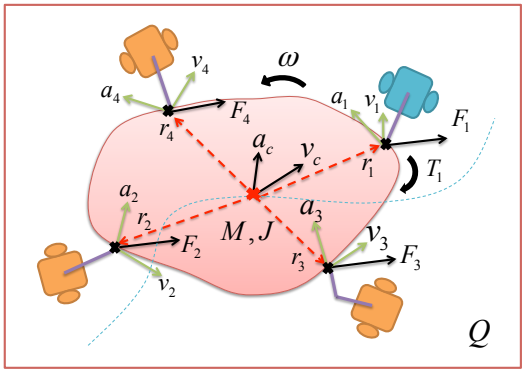

Figure 1. Visualization of a planar multi-robot (or "N-robot") manipulation task. The figure shows an example where four robots are manipulating an object. The robot in blue is the leader while the other robots in orange are followers.

Intuitively, from the perspective of a follower robot, the motion of the object contains indirect information about how other robots in the group apply their forces. We prove in this paper that this implicit information can be measured and used by individual robots to guarantee the convergence of the robots' forces to the leader's force. The object itself is used as a medium for transferring information throughout the robots.*

In a cooperative transport process by Force-ANTS, only the leader needs to be informed of the global position and desired trajectory of the object. The follower robots do not need to know where the object should go, where they themselves are, nor the control actions of other robots in the group. The leader can be either a robot or a human, as long as the leader can apply a force input to the object. This makes the Force-ANTS readily applicable to human-robot interaction and human-robot cooperative manipulation. Force-ANTS has many applications in real-life scenarios where large objects or assemblies need to be transported autonomously or under the guidance of a human operator. For example, in an automated construction site, heavy building material and building components can be transported by Force-ANTS. In a manufacturing facility, large parts and assemblies (e.g. for aircraft, trains, or industrial equipment) can be transported along various stages of the assembly line by Force-ANTS. In a disaster relief scenario, Force-ANTS can be used to clear large debris from a collapsed building and transport survivors to a safe place.

Some preliminary results from this paper appear in previous conference versions Wang and Schwager (2014, 2015, 2016). This paper has a series of contributions and improvements summarized as follows.

- Propose a unified Force-ANTS framework, which characterizes a class of controllers that deal with multi-robot manipulation without explicit communication.
- For two physics regimes, we prove that using our approach, the follower robots' forces converge to the leader's force, by measuring the object's motion as the only feedback.
- Provide proofs of convergence rates that the follower robots' forces converge to the leader's input force exponentially fast.
- Generalize our analysis to the case where follower robots can only measure the velocity and acceleration of the object at their local attachment points.
- Present hardware experiments with custom-built robots and simulation with up to 1000 robots that collectively transport a heavy piano.

Sec. 3 presents the unified Force-ANTS framework. Two implementations of Force-ANTS, namely Constant Boost Force-ANTS (CB-ANTS) and Proportional Force-ANTS (P-ANTS) are introduced in Sec. 4 and Sec. 5 respectively. For both implementations, we mathematically prove that the followers' forces will converge to the leader's force in Theorem 1 and Theorem 5, with the convergence rates characterized in Theorem 2 and Theorem 6 respectively. We also prove the effectiveness of Force-ANTS when the followers take heterogeneous local measurements of the object's motion in Theorem 3 and Theorem 7. Note that although we only analyze two kinds of Force-ANTS in this paper, more implementations are possible under the framework we propose. Both simulations and experiments are done to verify the Force-ANTS, in Sec 6 and 8 respectively, and the design of the proof-of-concept robots we build is explained in Sec. 7. Finally, conclusions and future work are given in Sec. 9.

2. Related Work

In terms of robotic manipulation, the seminal work by Khatib (1987) studied how to control the force on the end-effector of a manipulator, which is essential for approaches based on force feedback control like ours. More recently, there has been considerable attention on employing multiple robots to collectively manipulate a target object. The furniture moving problem was studied by Rus et al. (1995); Böhringer et al. (1997); Donald et al. (1997), where the tradeoff among different amount of sensing, communication and computation was discussed for the distributed manipulation process. Several works have considered a multi-robot manipulation solution called

*Note that although our approach discussed in this paper does not require a communication network, we do not prohibit the presence of a network. Indeed, if a network is present among the robots, it may be used for other planning and coordination purposes besides that described in this paper.

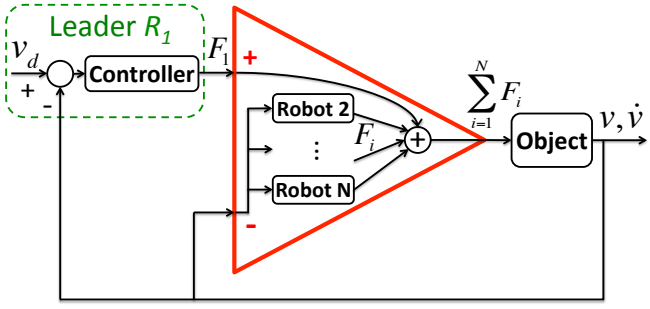

Figure 2. Block diagram of Force-ANTS framework. The leader applies its force $\mathbf{F}_1$ using a feedback controller to drive the object's velocity to the desired $\mathbf{v}_d$. The leader's force is amplified by the follower robots as they synchronize to the leader's force to move the object. The force synchronization requires no explicit communication. The followers take motion measurements of the object as the only feedback, as shown by the arrow into the inverting terminal of the amplifier.

caging Song and Kumar (2002); Wang and Kumar (2002); Pereira et al. (2004); Wan et al. (2012); Fink et al. (2008), where the robots move in a formation such that the object always stays inside the formation. Esposito (2009) proposed a force coordination approach for a robotic group based on the desired acceleration and a given communication network. An important issue in multi-robot manipulation is the impedance control (Erhart et al. (2013)), which can regulate internal forces (Williams and Khatib (1993); Khatib et al. (1999); Kennedy et al. (2015)) among multiple manipulators and reduce kinematic errors. Massive manipulation experiments were done by Becker et al. (2013) and Rubenstein et al. (2013) with about 100 robots using ensemble control or flocking. Habibi et al. (2015a,b) proposed a kinematic motion controller that coordinates a group of manipulation robots based on distributed centroid estimation of the object. Amanatiadis et al. (2015) managed to transport a real passenger vehicle using four omnidirectional robots, showing the strong capability of handling a large object with multiple robots. Another advantage of multi-robot manipulation is the handling of deformable object Alonso-Mora et al. (2015), which may be difficult for any individual manipulator. Ropes or cables were used as a tool to tow the object, by a group of ground robots Donald et al. (2000) or aerial robots Fink et al. (2011). Similar to our approach, some work focused on accomplishing the cooperative manipulation without communication. Most work within this scope use force sensors as an implicit means for coordination: Stilwell and Bay (1993) proposed an ant-like robot swarm system for object transport, where the follower robots track a leader by acting as passive casters; Kosuge and Oosumi (1996) let follower robots use force measurements to estimate the leader's intended trajectory; Groß and Dorigo (2004), Groß et al. (2006) and Baldassarre et al. (2007) developed a communication-free motion coordination controller for a group of physically connected robots using evolutionary algorithm using only inter-robot force measurements. Other than using force sensors, Chen et al. (2013) utilized visual occlusion to guide the robot swarm to move an object towards destination without communication, as verified by experiments in 2D and by simulations in 3D (Chen et al. (2015)). Passive robots also do not need communication when cooperating with a human to handle an object as shown by Hirata et al. (2008). None of the approaches above is fully decentralized, uses no communication and guarantees the efficiency of force alignment at the same time, which is achieved by our approach.

Our work is also related to multi-agent consensus, which serves as a tool in this paper to help us theoretically analyze the effectiveness of our controller. We are motivated by Olfati-Saber and Murray (2004); Jadbabaie et al. (2003) who studied the consensus algorithms that enable a group of agents or robots to agree on a common value by only having local communication with their neighbors. This agreed value of the group is steerable by introducing a leader agent Hong et al. (2006), and the controllability of this leader-following process was studied by Tanner (2004) and Ji et al. (2006).

We take some inspiration from the biological study of the collective transport or foraging in ants colony, whose behavior is very similar to the robots' defined in our paper. McCreery and Breed (2014) found the use of the object as an indirect media for information passing, and it was shown that ants can detect small-scale vibration or deformation of the object for motion coordination rather than communicating with other ants directly. The manipulation forces of the ant group are also shown to be coordinated during a object transport process, as measured by Berman et al. (2010). Wilson et al. (2014) designed a stochastic controller for swarm robots to emulate the measured ants behavior. Gelblum et al. (2015) discovered the leader-following mechanism in ant colony, where a small informed portion of ants actively lead and steer the whole group to the nest. All of these point to the biological plausibility of the method we describe in this paper.

3. Force-ANTS Framework

We consider the manipulation task in a 2D planar environment $Q \in \mathbb{R}^2$, as shown in Fig. 1. We have a group of N robots, indexed as $\{R_1, R_2, \cdots, R_N\}$. We specify R_1 as the leader robot and the rest as the follower robots. We assume that only the leader R_1 knows the desired trajectory while the followers have no information about where the object needs to go and all the robots are not allowed to communicate with each other.

Objective of Force-ANTS: take the leader's force as the input and generate a summed output force that aligns in the same direction as the input and has larger magnitude than the input force.

3.1. Force-ANTS Block Diagram

A block diagram that explains the Force-ANTS framework is shown in Figure 2. As can be seen in the figure, the core mission in implementing the Force-ANTS is to design a force controller for the follower robots, which will be given in later sections.

The Force-ANTS is analogous to the electrical amplifiers in many ways. They both amplify an input quantity to a greater output quantity, with an adjustable amplifying gain. They can both be modeled as a three-terminal component. Lastly, they both need a negative feedback of the output to the inverting terminal in order to stabilize the output.

3.2. Motion Initialization

The Force-ANTS becomes effective only when the object starts moving. Hence, an initial motion of the object must be triggered in the first place. This can be done without communication by random trials. When the object is stationary, all the robots apply random forces to the object. As time goes on, with probability one, there will be a time when the forces from the robots align well enough to overcome static friction. Once the object starts to move, the Force-ANTS will immediately take over and keep amplifying the leader's input to maintain the manipulation of the object. Although this paper does not treat the motion initialization phase in technical detail, in the Appendix (subsection C) we provide an analysis on estimating the number of random trials needed to overcome a given friction when the number of robots is large.

3.3. Translational Object Dynamics

Suppose that the object has a mass M and the acceleration of gravity is g. Denote the linear velocity of the object as $\mathbf{v}$. The 2D forces applied by the robots to the object are denoted by $\{\mathbf{F}_1, \mathbf{F}_2, \cdots, \mathbf{F}_N\}$. We model two kinds of drag forces. One is nonlinear kinetic friction with coefficient μ_k, which has a constant magnitude and always points opposite to the velocity of the object. The other one is linear viscous friction, which also points opposite to the velocity, but has a magnitude proportional to the velocity characterized by the coefficient μ_v.

The translational movement of the object is governed by Newton's second law. The specific drag force from the environment may differ depending on the task setup. As we humans do in real life, when the size of the object is moderate, it is often easier to directly push or pull the object on the ground and thus the kinetic friction dominates. In this case, the object dynamics can be written as

$$M\dot{\mathbf{v}} = \sum_{i=1}^{N} \mathbf{F}_i - \mu_k M g \frac{\mathbf{v}}{\|\mathbf{v}\|}, \tag{1}$$

or its discrete approximation by Euler's method:

$$M\frac{\mathbf{v}_{t+1} - \mathbf{v}_t}{\Delta t} = \sum_{i=1}^{N} \mathbf{F}_i(t) - \mu_k M g \frac{\mathbf{v}_t}{\|\mathbf{v}_t\|}. \tag{2}$$

In contrast, if the object is massive, it may be mounted on passive rollers, or mounted on top of the manipulation robots themselves. In this case, the dominating forces are the inertial forces of the object, and the viscous friction in the rolling device. Then the object dynamics is

$$M\dot{\mathbf{v}} = \sum_{i=1}^{N} \mathbf{F}_i - \mu_v \mathbf{v}. \tag{3}$$

Note that in practice, the robots compute their control laws and apply their forces in their local reference frames. However, we model the robots' forces in a global reference frame (which is not available to the follower robots) for the sake of analysis.

In order for the follower robots to make use of the motion measurements for force coordination, we assume that all the robots know the key parameters that determine the object dynamics, stated formally below.

Assumption 1. *All the robots know the value of* M, μ_k, μ_v, g, N.

Note that Assumption 1 can be achieved using existing distributed parameter estimation approaches, for example, by Franchi et al. (2015). Alternatively, adaptive control can be used, which is left for future work.

3.4. Rotation and Local Measurements

The proposed Force-ANTS only incorporates the translation velocity into the feedback loop. The rotation of the object will not be used for coordinating the follower robots, yet here we introduce a model to characterize and control the rotation. Suppose that the object's moment of inertia is J and the angular velocity is $\boldsymbol{\omega}$.

Assumption 2. *(Leader's Torque Input) In addition to applying a force, the leader can also measure the angular velocity of the object* $\boldsymbol{\omega}$ *and apply a direct torque to the object, denoted as* $\boldsymbol{T}_1$.

We inherit the model in our previous work (Wang and Schwager (2014)), that characterizes the damping from the environment as a linear torque, $-\mu_v J\boldsymbol{\omega}/M$. Then under Assumption 2, the rotational dynamics of the object is

$$J\dot{\boldsymbol{\omega}} = \mathbf{T}_1 + \sum_{i=1}^{N} \mathbf{r}_i \times \mathbf{F}_i - \frac{\mu_v}{M} J\boldsymbol{\omega}, \tag{4}$$

where $\mathbf{r}_i$ is the position vector pointing from the center of the mass to the attachment point of R_i.

Another issue that arises with rotation is the velocity and acceleration measurement. In practice the robots can only grasp the object at its perimeter, meaning that it is generally not possible to measure the velocity and acceleration at the center of the mass of the object, due to the lack of exact information on the geometry of the object. What the robots can actually measure are the velocities and accelerations at their local attachment points, denoted by x_i for R_i as shown in Figure 1. Then the difference between the local motion measurements and center of the mass measurement can be revealed in the following two equations,

$$\mathbf{v}_i = \mathbf{v}_c + \boldsymbol{\omega} \times \mathbf{r}_i, \tag{5}$$

$$\dot{\mathbf{v}}_i = \dot{\mathbf{v}}_c + \dot{\boldsymbol{\omega}} \times \mathbf{r}_i + \boldsymbol{\omega} \times (\boldsymbol{\omega} \times \mathbf{r}_i), \tag{6}$$

where $\mathbf{v}_i$ and $\dot{\mathbf{v}}_i$ denote the local motion measurements of the object by R_i while $\mathbf{v}_c$ and $\dot{\mathbf{v}}_c$ are the velocity and acceleration at the center of the mass of the object. The term, $\boldsymbol{\omega} \times (\boldsymbol{\omega} \times \mathbf{r}_i)$, is the centrifugal acceleration. Note that the Coriolis acceleration in our case is zero since the attachment point remains stationary in the object's local reference frame. As one can see, if the object rotates, then the motion measurements taken by different robots are all different, which presents a significant challenge to both the performance of the Force-ANTS and the theoretic analysis.

In the rest of the paper, we will show that both of our Force-ANTS implementations handle these local measurements well under some mild conditions. However, for the convenience of clearly conveying our idea, we will first introduce our controller based on the unrealistic homogeneous motion measurement at the center of the mass of the object. Then we will extend our controller to the heterogeneous local measurements case and prove the effectiveness of the force amplifier.

3.5. Centrosymmetric Robot Placement

We find that it often results in a performance improvement to place the robots around the object in a balanced way, as formalized in the following assumption.

Assumption 3. *(Centrosymmetric) The robots' attachment points are centrosymmetric around the center of mass of the object, meaning that for any robot i, there exists another robot $j \neq i$ such that $\boldsymbol{r}_i = -\boldsymbol{r}_j$.*

Although it is hard to achieve strict centrosymmetry without knowing the global geometry and position information, in realistic situations, when the number of robots is large with respect to the size of the object, it is likely that the robots will spread evenly around the object, so that Assumption 3 can be satisfied or nearly satisfied.

We require this assumption for our mathematical analysis, however we find experimentally that performance degrades gracefully as the assumption is violated. Intuitively, the benefit of this assumption is that it reduces the complexity in the rotational dynamics. Specifically, when all the forces from the robots are equal, the resultant torque (second term in (4)) generated by robots' forces will be zero, as shown in Figure 3.

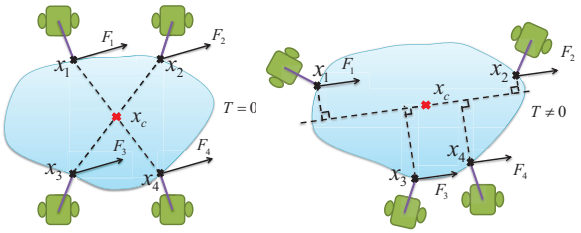

Figure 3. A comparison of the effect on rotation dynamics between centrosymmetric (left) and non-centrosymmetric (right) configurtion.

The second benefit of the centrosymmetry is the reduction of disturbance when using the local measurements, which will be discussed in detail for both CB-ANTS in Sec. 4.5 and P-ANTS in Sec. 5.4.

4. Constant Boost Force-ANTS

In this section, we introduce our first Force-ANTS implementation, which is designed for the scenario where the kinetic friction is the only drag force from the ground. As the name indicates, the Constant Boost Force-ANTS (CB-ANTS) is essentially nonlinear in that it will output a boost force of a constant magnitude, which is $(N-1)\mu_k Mg/N$, along the direction of the leader's force in the steady state regardless of the input magnitude. We define the boost force as the sum of all the followers' forces. It is therefore not surprising to envision that the follower's feedback controller is also nonlinear since it will deal with the nonlinear kinetic friction. In the rest of this section, we will present the design of the follower's controller based on the object dynamics (1), (2) and then prove the effectiveness of the CB-ANTS using either the simplified measurement at the center of the mass of the object, or the more practical local measurements at the attachment points.

4.1. Follower's Controller

The follower's controller we design uses only the measurement of the object's velocity in order to amplify the leader's input force. The principle of the controller is to let every follower robot apply its force along the direction of the velocity of the object with a magnitude of $1/N$ share of the total friction that needs to be overcome. The controller

can be formally written as

$$\mathbf{F}_i^i = \frac{\mu_k M g}{N} \frac{\mathbf{v}^i}{\|\mathbf{v}^i\|},\ i = \{2, 3, \cdots, N\}, \tag{7}$$

where the superscript i denotes the reference frame of robot i, since there is no global reference frame information, and the robots only know their local reference frames. For now we assume that the measurement $\mathbf{v}^i$ represents the velocity of the object at the center of the mass, which will be extended to the local measurement case later. Note that the controller (7) itself shows that no communication is needed among the robots.

Before the rigorous proof, the intuitive explanation behind the follower's controller is as follows. The velocity of the object contains necessary information about the leader's input force. By applying their forces along the velocity of the object, the followers provide the trend to maintain the object's motion such that the leader does not need to exert an extremely large force. On the other hand, the leader's change on its force will be reflected by the change of the object's velocity, which can be sensed by the followers in order to adjust their forces accordingly. In such a process, the followers can follow the leader and keep amplifying the leader's force without stopping the object.

4.2. Leader's Controller

The leader wants to steer the object to a desired destination or trajectory by applying a force which will be amplified by the followers. The design of the leader's controller is more flexible than the followers', as long as it can reduce the error between the object's actual velocity and desired velocity given by the higher-level path planning algorithm. The controller we choose is as follows,

$$\mathbf{F}_1^1 = f_d \frac{\mathbf{v}_d^1}{\|\mathbf{v}_d^1\|}, \tag{8}$$

where $\mathbf{v}_d^1$ is the desired velocity of the object expressed in the leader's local reference frame and f_d is a scalar determined by

$$f_d = K_p \max\{\|\mathbf{v}_d^1\| - \|\mathbf{v}^1\|, 0\}. \tag{9}$$

The underlying principle in determining $\mathbf{F}_1$ is to drive the object towards the desired velocity $\mathbf{v}_d^1$. From equation (8) we can see that $\mathbf{F}_1$ has the same direction as $\mathbf{v}_d^1$ while the magnitude is governed by a proportional controller that tends to reduce the difference between the magnitude of $\mathbf{v}_d^1$ and $\mathbf{v}^1$. The $\max$ function is used to ensure that $\mathbf{F}_1$ does not point opposite to $\mathbf{v}_d^1$.

4.3. Convergence Proof of the CB-ANTS

Putting the object dynamics and robots' forces together, here we study whether the CB-ANTS can successfully generate a boost force of constant magnitude $(N-1)\mu_k Mg/N$ along the direction of the leader's input force in the steady state. Notice that the CB-ANTS is nonlinear, making the traditional analysis difficult. Here we present our vector-based proof in the discrete time domain. The main proof of the CB-ANTS relies on the lemma below.

Lemma 1. *Given a constant vector $\boldsymbol{w}$, update vector $\boldsymbol{v}$ using the following discrete formula,*

$$\boldsymbol{v}_{t+1} = \alpha_t \boldsymbol{w} + \beta_t \boldsymbol{v}_t,$$

where $\{\alpha_t | \alpha_t \geqslant 0, \alpha_0^2 + \alpha_1^2 + \cdots + \alpha_t^2 \neq 0\}$ is a series of non-negative constants, and $\{\beta_t | 0 < \beta_t < 1\}$ is a series of constants between 0 and 1. Then the direction of $\boldsymbol{v}_t$ will converge to the direction of $\boldsymbol{w}$ as $t \to +\infty$, i.e.,

$$\boldsymbol{v}_t \to \gamma \boldsymbol{w},$$

where $\gamma > 0$ is a scalar determined by $\{\alpha_t\}$ and $\{\beta_t\}$.

Proof. Starting from $t = 0$, we have

$$\mathbf{v}_1 = \alpha_0 \mathbf{w} + \beta_0 \mathbf{v}_0,$$

$$\mathbf{v}_2 = \alpha_1 \mathbf{w} + \beta_1 \mathbf{v}_1 = (\alpha_1 + \beta_1 \alpha_0)\mathbf{w} + \beta_0 \beta_1 \mathbf{v}_0,$$

$$\mathbf{v}_3 = \alpha_2 \mathbf{w} + \beta_2 \mathbf{v}_2 = (\alpha_2 + \beta_2 \alpha_1 + \beta_2 \beta_1 \alpha_0)\mathbf{w} + \beta_0 \beta_1 \beta_2 \mathbf{v}_0.$$

By induction, we further have

$$\begin{aligned}\mathbf{v}_t = (&\alpha_{t-1} + \beta_{t-1}\alpha_{t-2} + \beta_{t-1}\beta_{t-2}\alpha_{t-3} + \cdots + \\ &\beta_{t-1}\beta_{t-2}\cdots\beta_2\beta_1\alpha_0)\mathbf{w} + (\beta_0\beta_1\cdots\beta_{t-2}\beta_{t-1})\mathbf{v}_0.\end{aligned}$$

As $t \to +\infty$, we know $\beta_0\beta_1\beta_2\cdots\beta_{t-2}\beta_{t-1} \to 0$. Therefore,

$$\mathbf{v}_t \to \gamma \mathbf{w},$$

where

$$\begin{aligned}\gamma = &\alpha_{t-1} + \beta_{t-1}\alpha_{t-2} + \beta_{t-1}\beta_{t-2}\alpha_{t-3} + \cdots + \\ &\beta_{t-1}\beta_{t-2}\cdots\beta_2\beta_1\alpha_0.\end{aligned} \tag{10}$$

Apparently $\gamma > 0$, so $\mathbf{v}_t$ and $\mathbf{w}$ have the same direction, and this completes the proof. □

Theorem 1. *(CB-ANTS) Given the CB-ANTS described by Figure 2 and Eq. (2), (7), (8), when the time step satisfies $0 < \Delta t < N\|\boldsymbol{v}_t\|/\mu_k g$, the CB-ANTS will output a boost force of constant magnitude $(N-1)\mu_k Mg/N$ aligning in the same direction as the leader's force in the steady state. The object's velocity will also converge to the desired velocity $\boldsymbol{v}_d$.*

Proof. Since the follower's controller sets the magnitude of the each follower's force to be $\mu_k Mg/N$ by construction, the proof will mainly focus on the convergence of the direction of the follower's force to the leader's force. We

will prove the theorem in the discrete time domain, and assume that all controllers and dynamics are updated in synchronized time steps. Rewriting equation (7), (8) in the world frame, we get

$$\mathbf{F}_i(t) = \frac{\mu_k M g}{N}\frac{\mathbf{v}_t}{\|\mathbf{v}_t\|},\ i = \{2, 3, \cdots, N\}, \tag{11}$$

$$\mathbf{F}_1(t) = K_p \max\{\|\mathbf{v}_d\| - \|\mathbf{v}_t\|, 0\}\frac{\mathbf{v}_d}{\|\mathbf{v}_d\|}. \tag{12}$$

Note that we remove the superscript i on all the $\mathbf{v}$ because we express all the quantities in the world reference frame throughout this proof for the convenience of analysis. This does not affect the correctness of the proof since all the $\mathbf{v}_t^i$ are actually the same vector, although they may be different in different local reference frames. Plug (11), (12) into (2) and we have

$$\begin{aligned}\mathbf{v}_{t+1} &= \mathbf{v}_t + \frac{\Delta t}{M}\left(\mathbf{F}_1(t) + (N-1)\frac{\mu_k M g}{N}\frac{\mathbf{v}_t}{\|\mathbf{v}_t\|}\right) \\ &\quad - \mu_k g \Delta t \frac{\mathbf{v}_t}{\|\mathbf{v}_t\|} \\ &= \frac{K_p \max\{\|\mathbf{v}_d\| - \|\mathbf{v}_t\|, 0\}\Delta t}{M\|\mathbf{v}_d\|}\mathbf{v}_d + \left(1 - \frac{\mu_k g \Delta t}{N\|\mathbf{v}_t\|}\right)\mathbf{v}_t\end{aligned} \tag{13}$$

Then we can use the conclusion in Lemma 1 by letting

$$\alpha_t = \frac{K_p \max\{\|\mathbf{v}_d\| - \|\mathbf{v}_t\|, 0\}\Delta t}{M\|\mathbf{v}_d\|} \geqslant 0,$$

$$0 < \beta_t = 1 - \frac{\mu_k g \Delta t}{N\|\mathbf{v}_t\|} < 1, \tag{14}$$

which are true when $\Delta t < N\|\mathbf{v}_t\|/\mu_k g$. Therefore we know that the direction of $\mathbf{v}_t$ will converge to that of $\mathbf{v}_d$. Then by summing up all the followers' forces, we get that the boost force CB-ANTS provides will converge to

$$\sum_{i=2}^{N}\mathbf{F}_i \to \frac{N-1}{N}\mu_k M g \frac{\mathbf{v}_d}{\|\mathbf{v}_d\|},$$

which has a constant magnitude $(N-1)\mu_k Mg/N$ and aligns with the leader's input force.

In addition, the magnitude of $\mathbf{v}_t$ will also converge to $\mathbf{v}_d$ because the magnitude is decoupled from the direction and is governed by a proportional controller. As a result, the followers' forces will align with the leader's according to (11) when $\mathbf{v}_t \to \mathbf{v}_d$. □

Remark 1. Theorem 1 shows that CB-ANTS can successfully amplify the leader's force by providing a boost force on top of the leader's force, which accounts for $\frac{N-1}{N}$ share of the total friction. However, the leader may need to apply a force slightly larger than $\mu_k Mg/N$ in order to steer the object. This happens when the leader suddenly changes the direction of its force so that the followers' forces do not align with the leader's temporarily. In this case, the leader needs to apply a force larger than $1/N$ of the friction to make sure the sum force can overcome friction. In other words, the acceleration (either speeding up or slowing down) of the object is controlled by the leader.

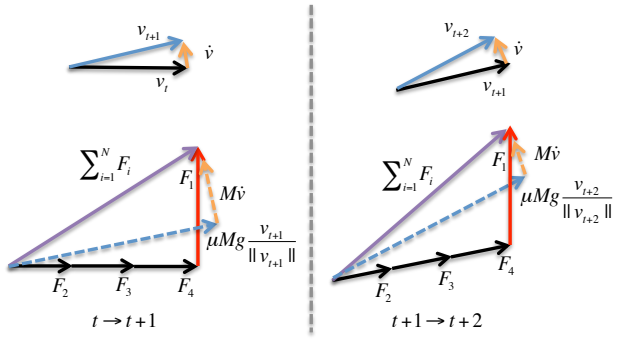

Figure 4. Geometric explanation of Theorem 1. The evolution from t to $t+2$ with 1 leader and 3 follower robots is shown. It can be seen that if $\mathbf{F}_1$ sticks with its direction all the time, then graudually $\mathbf{v}$ and $\mathbf{F}_i$ will converge to the direction of $\mathbf{F}_1$.

Remark 2. The evolution of the force alignment is also visualized in Figure 4 by showing an example from time t to $t+2$. We find that the condition on Δt is easily satisfied in practice with an update rate of 100Hz.

4.4. Convergence Rate of CB-ANTS

We provide the analysis of convergence rate for Theorem 1 in this section. In the CB-ANTS case, we evaluate the convergence rate in terms of how fast the direction of any follower's force can synchronize to the leader's input force. The conclusion is that the convergence rate is exponential, as shown in the theorem below.

Theorem 2. *(CB-ANTS convergence rate) In CB-ANTS, the direction of any follower's force will converge to the leader's input force exponentially fast.*

Proof. We can propagate the dynamics in (13) to the initial velocity $\mathbf{v}_0$, as was done in Lemma 1,

$$\mathbf{v}_t - \gamma\mathbf{v}_d = (\beta_0\beta_1\cdots\beta_{t-2}\beta_{t-1})\mathbf{v}_0, \tag{15}$$

where γ and β_t can be determined by (10) and (14). Then let

$$\beta_m = \max\{\beta_0, \beta_1, \cdots, \beta_{t-1}\},$$

we have

$$\|\mathbf{v}_t - \gamma\mathbf{v}_d\| \leq \beta_m^t\|\mathbf{v}_0\|. \tag{16}$$

Since $0 < \beta_m < 1$, according to the definition of exponential stability for discrete-time systems by Lakshmikantham et al. (1988) and Aitken and Schwartz (1994), (16) indicates

that $\mathbf{v}_t$ converges to $\gamma \mathbf{v}_d$ exponentially fast. Since the followers' forces have the same direction as $\mathbf{v}_t$ and the leader's force has the same direction as $\mathbf{v}_d$, we know that the direction of the followers' forces will converge to the leader's force exponentially fast. □

4.5. CB-ANTS with Local Measurements

Now we extend Theorem 1 to the case where the follower robots use local motion measurements as shown in (5). Our conclusion is that Theorem 1 still holds with heterogeneous local measurements if the magnitude of the angular velocity can be linearly bounded by the magnitude of the translational velocity. Furthermore, we will analyze how the centrosymmetric configuration of the robots (Assumption 3) can help reduce disturbance in this case.

Using the local measurement, the follower's controller becomes

$$\mathbf{F}_i = \frac{\mu_k M g}{N} \frac{\mathbf{v}_t + \boldsymbol{\omega}_t \times \mathbf{r}_i}{\|\mathbf{v}_t + \boldsymbol{\omega}_t \times \mathbf{r}_i\|}. \tag{17}$$

The leader's controller remains the same as (8). Then plugging all robots' forces into the object dynamics yields

$$\begin{aligned}
\mathbf{v}_{t+1} &= \mathbf{v}_t + \frac{\Delta t}{M} \sum_{i=1}^{N} \mathbf{F}_i(t) - \mu_k g \Delta t \frac{\mathbf{v}_t}{\|\mathbf{v}_t\|} \\
&= \frac{\Delta t}{M} f_d \frac{\mathbf{v}_d}{\|\mathbf{v}_d\|} + \frac{\mu_k g \Delta t}{N} \sum_{i=2}^{N} \frac{\mathbf{v}_t + \boldsymbol{\omega}_t \times \mathbf{r}_i}{\|\mathbf{v}_t + \boldsymbol{\omega}_t \times \mathbf{r}_i\|} \\
&\quad + \left(1 - \frac{\mu_k g \Delta t}{\|\mathbf{v}_t\|}\right) \mathbf{v}_t \\
&= \frac{\Delta t}{M} f_d \frac{\mathbf{v}_d}{\|\mathbf{v}_d\|} + \sum_{i=2}^{N} \left(\frac{\mu_k g \Delta t}{N \|\mathbf{v}_t + \boldsymbol{\omega}_t \times \mathbf{r}_i\|}\right) \boldsymbol{\omega}_t \times \mathbf{r}_i + \\
&\quad + \left(1 + \sum_{i=2}^{N} \frac{\mu_k g \Delta t}{N \|\mathbf{v}_t + \boldsymbol{\omega}_t \times \mathbf{r}_i\|} - \frac{\mu_k g \Delta t}{\|\mathbf{v}_t\|}\right) \mathbf{v}_t
\end{aligned} \tag{18}$$

In the above equation, the first term is the control input of the leader robot. The second term is the disturbing term along the tangential directions at robots' attachment points around the object. The last term denotes the internal dynamics of the object's velocity. Our motivation is that we want the coefficient of the internal dynamics to be less than 1, so that the internal dynamics is stable. We also need to keep the second disturbing term small so that we can reject the disturbance using the PI controller of the leader.

Theorem 3. *(CB-ANTS Local) When the follower robots use the local measurements in (5), a sufficient condition for Theorem 1 to hold is*

$$\|\boldsymbol{\omega}_t\| < \frac{\|\boldsymbol{v}_t\|}{N \|\boldsymbol{r}_m\|}, \tag{19}$$

where $m = \operatorname{argmax}_{\{i=2,\cdots,N\}} \|\boldsymbol{r}_i\|$.

Proof. Consider the third term in (18), if (19) is satisfied, then we have

$$\begin{aligned}
\sum_{i=2}^{N} \frac{\mu_k g \Delta t}{N \|\mathbf{v}_t + \boldsymbol{\omega}_t \times \mathbf{r}_i\|} &\leq \sum_{i=2}^{N} \frac{\mu_k g \Delta t}{N(\|\mathbf{v}_t\| - \|\boldsymbol{\omega}_t \times \mathbf{r}_i\|)} \\
&\leq \sum_{i=2}^{N} \frac{\mu_k g \Delta t}{N(\|\mathbf{v}_t\| - \|\boldsymbol{\omega}_t \times \mathbf{r}_m\|)} \\
&< \sum_{i=2}^{N} \frac{\mu_k g \Delta t}{(N-1)\|\mathbf{v}_t\|} = \frac{\mu_k g \Delta t}{\|\mathbf{v}_t\|}.
\end{aligned}$$

Therefore we have

$$\left(1 + \sum_{i=2}^{N} \frac{\mu_k g \Delta t}{N \|\mathbf{v}_t + \boldsymbol{\omega}_t \times \mathbf{r}_i\|} - \frac{\mu_k g \Delta t}{\|\mathbf{v}_t\|}\right) < 1.$$

Then we can apply Lemma 1 to derive the convergence of $\mathbf{v}_t \to \mathbf{v}_d$. The disturbing term in (18) can be rejected through a PI controller by the leader. Actually, the magnitude of the disturbance is also bounded if (19) is satisfied, as shown below

$$\begin{aligned}
&\left\| \sum_{i=2}^{N} \left(\frac{\mu_k g \Delta t}{N \|\mathbf{v}_t + \boldsymbol{\omega}_t \times \mathbf{r}_i\|}\right) \boldsymbol{\omega}_t \times \mathbf{r}_i \right\| \\
&\qquad < \sum_{i=2}^{N} \left(\frac{\mu_k g \Delta t}{(N-1)\|\mathbf{v}_t\|}\right) \frac{\|\mathbf{v}_t\|}{N} = \frac{\mu_k g \Delta t}{N}.
\end{aligned} \tag{20}$$

The bound in (20) indicates that the magnitude of the disturbance is smaller than the capacity of the leader's maximal force input. Having $\mathbf{v}_t \to \mathbf{v}_d$, the rest of the argument will be the same as Theorem 1. □

Remark 1. Theorem 3 provides a sufficient condition, and it may be very conservative. Depending on the geometric distribution of the robots around the object, the velocity convergence may still hold when the magnitude of $\boldsymbol{\omega}$ violates the bound in (19). Eq. (19) can be used as a guideline or reference to reduce rotation in order to get better control on the translational motion. In practice, the angular velocity can be limited or reduced in many ways, for example, by the physical constraints of the robots (not able to move sideways), or by utilizing the leader's direct torque input as shown in (4).

Remark 2. Intuitively, the rotation will cause the followers to apply part of their forces along the tangential direction at their attachment points and lose magnitude along the translational direction since all the followers apply a force with a fixed magnitude. If the linear velocity associated with rotation $\boldsymbol{\omega} \times \mathbf{r}_i$ is large enough to overcome $\mathbf{v}_t$, then the follower robot will get no information about where the object is being navigated to by measuring the

local velocity, and will then point its force to a meaningless direction.

Remark 3. Considering (20), in the worst scenario the disturbance is bounded by $\mu_k Mg/N$. Although the worst case is unlikely to happen in the real time (which requires all the robots gather at the same attachment point and $\mathbf{v}_t$, $\boldsymbol{\omega}_t \times \mathbf{r}_i$ have the opposite direction), it is beneficial for the leader robot to have a larger force capacity than $\mu_k Mg/N$, leaving more margin to reject the disturbance.

Remark 4. The proof of Theorem 3 does not require the centrosymmetric assumption. However, having the centrosymmetry property will result in a tighter bound on the disturbance than (20). Theorem 4 below quantitatively characterizes this disturbance rejection by introducing the centrosymmetric configuration.

Theorem 4. *(CB-ANTS Disturbance Bound) Under Assumption 3, condition (19) and when $N > 3$, the disturbance term in (18) is bounded by*

$$\left\| \sum_{i=2}^{N} \left(\frac{\mu_k g \Delta t}{N \|\boldsymbol{v}_t + \boldsymbol{\omega}_t \times \boldsymbol{r}_i\|} \right) \boldsymbol{\omega}_t \times \boldsymbol{r}_i \right\| < \frac{\mu_k g \Delta t}{N} \left(\frac{2N-1}{N^2-N} \right).$$

Proof. The disturbance term is a sum of $N-1$ terms. According to the centrosymmetric assumption, among the $N-1$ terms we can find $(N-2)/2$ paired terms associated with paired robots, and one singular term (indexed as k) that does not have a pair. For every paired terms who have the position vector $\mathbf{r}_i$ and $-\mathbf{r}_i$, we can calculate the sum of them,

$$\begin{aligned}
&\left(\frac{\mu_k g \Delta t}{N \|\mathbf{v}_t + \boldsymbol{\omega}_t \times \mathbf{r}_i\|} \right) \boldsymbol{\omega}_t \times \mathbf{r}_i + \left(\frac{\mu_k g \Delta t}{N \|\mathbf{v}_t - \boldsymbol{\omega}_t \times \mathbf{r}_i\|} \right) \boldsymbol{\omega}_t \times (-\mathbf{r}_i) \\
&= \frac{\mu_k g \Delta t}{N} \boldsymbol{\omega}_t \times \mathbf{r}_i \left(\frac{1}{\|\mathbf{v}_t + \boldsymbol{\omega}_t \times \mathbf{r}_i\|} - \frac{1}{\|\mathbf{v}_t - \boldsymbol{\omega}_t \times \mathbf{r}_i\|} \right) \\
&\leq \frac{\mu_k g \Delta t}{N} \boldsymbol{\omega}_t \times \mathbf{r}_i \left(\frac{1}{\|\mathbf{v}_t\| - \|\boldsymbol{\omega}_t \times \mathbf{r}_i\|} - \frac{1}{\|\mathbf{v}_t\| + \|\boldsymbol{\omega}_t \times \mathbf{r}_i\|} \right) \\
&\leq \frac{\mu_k g \Delta t}{N} \boldsymbol{\omega}_t \times \mathbf{r}_i \left(\frac{1}{\|\mathbf{v}_t\| - \|\boldsymbol{\omega}_t \times \mathbf{r}_m\|} - \frac{1}{\|\mathbf{v}_t\| + \|\boldsymbol{\omega}_t \times \mathbf{r}_m\|} \right) \\
&\leq \frac{\mu_k g \Delta t}{N} \boldsymbol{\omega}_t \times \mathbf{r}_i \left(\frac{N}{(N-1)\|\mathbf{v}_t\|} - \frac{N}{(N+1)\|\mathbf{v}_t\|} \right) \\
&\leq \frac{\mu_k g \Delta t}{N} \boldsymbol{\omega}_t \times \mathbf{r}_i \frac{2N}{\|\mathbf{v}_t\|(N^2-1)}.
\end{aligned}$$

For the singular term associated with $\mathbf{r}_k$, it is bounded by

$$\begin{aligned}
&\left(\frac{\mu_k g \Delta t}{N \|\mathbf{v}_t + \boldsymbol{\omega}_t \times \mathbf{r}_k\|} \right) \boldsymbol{\omega}_t \times \mathbf{r}_k \leq \\
&\frac{\mu_k g \Delta t}{N} \boldsymbol{\omega}_t \times \frac{\mathbf{r}_k}{\|\mathbf{v}_t\| - \|\boldsymbol{\omega}_t \times \mathbf{r}_k\|} \leq \frac{\mu_k g \Delta t}{N} \boldsymbol{\omega}_t \times \frac{N \mathbf{r}_k}{(N-1)\|\mathbf{v}_t\|}
\end{aligned}$$

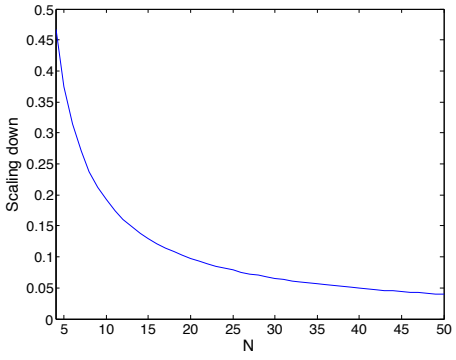

Figure 5. Plot of the scaling factor $(2N-1)/(N^2-N)$ when N goes from 4 to 50.

Then putting all $N-1$ terms together we have

$$\begin{aligned}
&\left\| \sum_{i=2}^{N} \left(\frac{\mu_k g \Delta t}{N \|\mathbf{v}_t + \boldsymbol{\omega}_t \times \mathbf{r}_i\|} \right) \boldsymbol{\omega}_t \times \mathbf{r}_i \right\| \leq \\
&\frac{\mu_k g \Delta t}{N} \|\boldsymbol{\omega}_t \times \mathbf{r}_m\| \left(\frac{N-2}{2} \cdot \frac{2N}{\|\mathbf{v}_t\|(N^2-1)} + \frac{N}{\|\mathbf{v}_t\|(N-1)} \right) \\
&\leq \frac{\mu_k g \Delta t}{N} \left(\frac{2N-1}{N^2-N} \right). \qquad \square
\end{aligned}$$

It can be seen from Theorem 4 that the disturbance under the centrosymmetric assumption is scaled down by $(2N-1)/(N^2-N)$. Moreover, this scaling factor decreases monotonically as N gets larger. Figure 5 plots the value of the scaling factor when N ranges from 4 to 50. As shown in the figure, when N reaches 20, the magnitude of the disturbance already falls down below 10% of the original bound in (20).

5. Proportional Force-ANTS

In this section, we present our second Force-ANTS implementation, Proportional Force-ANTS (P-ANTS), for the scenario where viscous friction is the only drag force. We therefore base our analysis in this section on the object dynamics (3). Compared to CB-ANTS, the object considered in P-ANTS can have much larger scale such that the inertial force and viscous force are more significant than kinetic friction.

P-ANTS not only tracks the direction of the leader's force, but also generates an output force whose magnitude is proportional to the leader's input force, and the amplifying gain of P-ANTS is N. In order to be able to steer the magnitude, P-ANTS also needs the follower robots to measure the acceleration of the object, in addition to the velocity measurement as in CB-ANTS.

We take some inspiration from the consensus-based leader following (Olfati-Saber and Murray (2004)) when designing the follower's controller and use consensus as a

tool to prove the stability of the force coordination. When the followers use the center of the mass measurements, P-ANTS is completely linear and can be described as a first-order linear system. In contrast, using the heterogeneous local measurements will introduce nonlinearity to the system and we will prove the stability using the Lyapunov arguments.

5.1. Consensus-based Force Coordination

In P-ANTS, the force of every follower robot will converge to the leader's force, in the sense of both direction and magnitude. This can be done without communication using the follower's force controller below,

$$\dot{\mathbf{F}}_i = \sum_{j=1, j\neq i}^{N} (\mathbf{F}_j - \mathbf{F}_i) = \sum_{j=1}^{N} \mathbf{F}_j - N\mathbf{F}_i \tag{21}$$

$$= M\dot{\mathbf{v}} + \mu_v \mathbf{v} - N\mathbf{F}_i. \tag{22}$$

Remarkably, equation (21) is an implementation of a well known consensus law (Olfati-Saber and Murray (2004)) and will lead to all robots applying equal force vectors to the object. In a normal consensus protocol, each robot i needs to communicate with its neighbors to get $\mathbf{F}_j$. However in our case, the sum of all unknown $\mathbf{F}_j$ plus robot i's own force is a known quantity by (3) given that robots can measure $\dot{\mathbf{v}}$ and $\mathbf{v}$. Hence the consensus control law can be computed using (22) without communication.

Furthermore, it was also proven by Olfati-Saber and Murray (2004) that if there is one leader agent who does not change its value, then the values of all other agents in the network will converge to the leader's value. The following proposition can be concluded using this result.

Proposition 1. *In P-ANTS, given a static leader who sticks with its initial force $\boldsymbol{F}_1(0)$ all the time, then using the controller (22), all the followers' forces will converge to the leader's force, i.e.,*

$$\lim_{t\to\infty} \boldsymbol{F}_i(t) = \boldsymbol{F}_1(0),\ i \in \{2, 3, \cdots, N\}. \tag{23}$$

Proof. Refer to Olfati-Saber and Murray (2004). □

In addition, we know that P-ANTS can amplify the leader's input force with an amplifying gain N since $\sum_{i=1}^{N} \mathbf{F}_i \to N\mathbf{F}_1$.

5.2. Dynamical Characterization of P-ANTS

The result in Proposition 1 only reflects the followers' convergence to a stationary leader. We are also interested in the dynamical behavior of P-ANTS with respect to a changing leader. Treat the leader's input force as the input and the total force from all the robots as the output, then P-ANTS can be put into a standard state-space form, as shown in the following theorem.

Theorem 5. *(P-ANTS) Given the P-ANTS described by Figure 2 and (3), (22), then the dynamics between the leader's input force and the amplified group output force can be written as follows,*

$$\begin{aligned} \dot{\boldsymbol{\eta}} &= -\boldsymbol{\eta} + \boldsymbol{F}_1 \\ \boldsymbol{F}_s &= (N-1)\boldsymbol{\eta} + \boldsymbol{F}_1 \end{aligned} \tag{24}$$

where $\boldsymbol{F}_s = \sum_{i=1}^{N} \boldsymbol{F}_i$ is the group force, and $\boldsymbol{\eta} = (\sum_{i=2}^{N} \boldsymbol{F}_i)/(N-1)$ denotes the average force of all followers.

Proof. By adding up (22) when i goes from 2 to N we have

$$\begin{aligned} \sum_{i=2}^{N} \dot{\mathbf{F}}_i &= (N-1)\sum_{j=1}^{N} \mathbf{F}_j - N\sum_{i=2}^{N} \mathbf{F}_i \\ &= (N-1)\sum_{j=1}^{N} \mathbf{F}_j - N\left(\sum_{j=1}^{N} \mathbf{F}_j - \mathbf{F}_1\right) \\ &= -\sum_{j=1}^{N} \mathbf{F}_j + N\mathbf{F}_1 = -\sum_{j=2}^{N} \mathbf{F}_j + (N-1)\mathbf{F}_1. \end{aligned}$$

Hence by dividing $N-1$ on both sides we have $\dot{\boldsymbol{\eta}} = -\boldsymbol{\eta} + \mathbf{F}_1$, and $\mathbf{F}_s = (N-1)\boldsymbol{\eta} + \mathbf{F}_1$ since $\mathbf{F}_s$ is the sum of followers' forces and the leader's force. □

Remark 1. Knowing the exact linear dynamics, we can implement a feedback controller for the leader's force $\mathbf{F}_1$ in order to steer the group force with desired specifications. The input-output dynamics and the force amplifying gain is more clear in the transfer function form, which can be acquired by taking the Laplace transformation of (24),

$$\frac{\mathbf{F}_s(s)}{\mathbf{F}_1(s)} = \frac{s+N}{s+1}. \tag{25}$$

It follows immediately that the steady state gain is N as $s \to 0$ using the finite value theorem. Also, P-ANTS has an equivalent electrical counterpart as shown in Figure 6. The connection between P-ANTS and very well-known dynamical systems makes it applicable to use traditional controller design techniques, such as the frequency domain methods, to specify the proper leader's controller for the input force.

Remark 2. In (24) and (25), all the vectors are 2D. However, the x and y component are independent, so we do not distinguish them repeatedly.

5.3. Convergence Rate of P-ANTS

We provide the analysis of convergence rate for Theorem 5 in this section. The convergence rate is defined similarly as in Section 4.4, with the only difference that we take into account both magnitude and direction in the P-ANTS

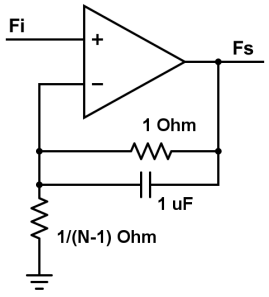

Figure 6. Equivalent electrical amplifier circuits of P-ANTS. This electrical amplifier has the same transfer function as P-ANTS. In both the electrical amplifier and P-ANTS, the amplifying gain is configurable by changing the value of N.

case. The conclusion is again exponential convergence, as revealed in Lemma 2 and Theorem 6 below.

Lemma 2. *The difference between any two follower robots' forces using controller (22) will converge exponentially to zero regardless of the leader's input. The rate of this exponential convergence increases linearly with the number of robots.*

Proof. Consider any two follower robots R_i and R_k, according to (21)

$$\dot{\mathbf{F}}_i - \dot{\mathbf{F}}_k = -N(\mathbf{F}_i - \mathbf{F}_k).$$

So we have

$$\mathbf{F}_i - \mathbf{F}_k = \mathbf{C}_{ik} e^{-Nt}, \tag{26}$$

where $\mathbf{C}_{ik}$ is a constant depending on the initial condition. □

Theorem 6. *(P-ANTS convergence rate) Using controller (22) and if the leader's force is constant, any follower's force will converge to the leader's force exponentially fast with a constant rate.*

Proof. From (21) and (26) we know for any $i \in \{2, 3, \cdots, N\}$,

$$\begin{aligned}\dot{\mathbf{F}}_i &= (\mathbf{F}_1 - \mathbf{F}_i) + \sum_{j=2, j\neq i}^{N} (\mathbf{F}_j - \mathbf{F}_i) \\ &= -\mathbf{F}_i + \mathbf{F}_1 + \sum_{j=2, j\neq i}^{N} \mathbf{C}_{ji} e^{-Nt}. \end{aligned} \tag{27}$$

Given that $\mathbf{F}_1$ is a constant, (27) is a first-order non-homogeneous differential equation in terms of $\mathbf{F}_i$, whose solution can be written down explicitly as follows,

$$\mathbf{F}_i = \mathbf{F}_1 + \mathbf{C}_i e^{-t} + \sum_{j=2, j\neq i}^{N} \left(-\frac{\mathbf{C}_{ji}}{N-1}\right) e^{-Nt},$$

where $\mathbf{C}_i$ can be determined by the initial condition. The equation above can be equivalently interpreted as

$$\mathbf{F}_i - \mathbf{F}_1 = \mathbf{C}_i e^{-t} + \sum_{j=2, j\neq i}^{N} \left(-\frac{\mathbf{C}_{ji}}{N-1}\right) e^{-Nt},$$

which indicates that the difference between the follower's and the leader's force will vanish to zero exponentially fast at a constant rate e^{-t}, since the terms with e^{-Nt} will fade away faster than e^{-t}. □

Remark 1. The result in Theorem 6 can still be valid when $\mathbf{F}_1$ is changing. In this case, instead of tracking an arbitrarily changing $\mathbf{F}_1$, we show that the followers can track a filtered $\mathbf{F}_1$,

$$\dot{\tilde{\mathbf{F}}}_1 = \mathbf{F}_1 - \tilde{\mathbf{F}}_1, \tag{28}$$

which can be seen as a "smoother" $\mathbf{F}_1$ generated by a first-order low-pass filter. Substitute (28) into (27) and resolve the differential equation, then we have

$$\mathbf{F}_i - \tilde{\mathbf{F}}_1 = \mathbf{C}_{i1} e^{-t} + \sum_{j=2, j\neq i}^{N} \left(-\frac{\mathbf{C}_{ji}}{N-1}\right) e^{-Nt}, \tag{29}$$

where $\mathbf{C}_{i1}$ and $\mathbf{C}_{ji}$ are constants determined by the initial condition. Clearly, (29) also implies exponential convergence of the followers' forces to the leader's.

5.4. P-ANTS with Local Measurements

We now proceed to address the problem of using local measurements in P-ANTS. More precisely, the unrealistic measurements $\dot{\mathbf{v}}$ and $\mathbf{v}$ in (22) will be replaced with the local measurement $\dot{\mathbf{v}}_i$ and $\mathbf{v}_i$, as follows,

$$\dot{\mathbf{F}}_i = M\dot{\mathbf{v}}_i + \mu_v \mathbf{v}_i - N\mathbf{F}_i, \; i \in \{2, 3, \cdots, N\}. \tag{30}$$

The goal here is to study the force convergence $\mathbf{F}_i \to \mathbf{F}_1$ using (30) so that the force amplification can still be achieved with a steady-state gain N. Our conclusion is that this is true under some mild geometric conditions (Assumption 3 and Eq. (35) below).

The heterogeneous local measurements, as characterized by (5), (6), bring significant nonlinearity to the consensus-based force coordination, which can be treated as a disturbance. To effectively reduce the disturbance and improve the system performance, we require Assumption 3 in the following analysis.

We start our convergence analysis of P-ANTS with local measurements by comparing its difference with the previous non-local one in (22). Using (3), (4), (5), (6) we

can write (30) as

$$\begin{aligned}\dot{\mathbf{F}}_i &= M\big(\dot{\mathbf{v}}_c + \dot{\boldsymbol{\omega}} \times \mathbf{r}_i + \boldsymbol{\omega} \times (\boldsymbol{\omega} \times \mathbf{r}_i)\big) + \\ &\quad \mu_v(\mathbf{v}_c + \boldsymbol{\omega} \times \mathbf{r}_i) - N\mathbf{F}_i \\ &= M\dot{\mathbf{v}}_c + \mu_v\mathbf{v}_c - N\mathbf{F}_i + M\boldsymbol{\omega} \times (\boldsymbol{\omega} \times \mathbf{r}_i) + \mu_v\boldsymbol{\omega} \times \mathbf{r}_i + \\ &\quad M(\frac{1}{J}\sum_{i=1}^{N}\mathbf{r}_i \times \mathbf{F}_i - \frac{\mu_v}{M}\boldsymbol{\omega}) \times \mathbf{r}_i \\ &= (\sum_{j=1}^{N}\mathbf{F}_j - N\mathbf{F}_i) + \frac{M}{J}(\sum_{j=1}^{N}\mathbf{r}_j \times \mathbf{F}_j) \times \mathbf{r}_i + \\ &\quad M\boldsymbol{\omega} \times (\boldsymbol{\omega} \times \mathbf{r}_i), \end{aligned} \tag{31}$$

where we exclude the reliance on the the leader's direct torque input by letting $\mathbf{T}_1 = 0$ in (4). The first term in (31) by itself would lead to a consensus, as in (21). The second and third terms in (31) appear as disturbances, denoting the additional effects caused by the rotation in the tangential and centrifugal directions. However, under Assumption 3, the centrifugal term $M\boldsymbol{\omega} \times (\boldsymbol{\omega} \times \mathbf{r}_i)$ in (31) will not have any influence on the consensus because it points towards the center of mass and will be canceled out by the paired symmetric robots. Hence, we only need to study the first two terms in (31), as follows

$$\dot{\mathbf{F}}_i = (\sum_{j=1}^{N}\mathbf{F}_j - N\mathbf{F}_i) - \frac{M}{J}\mathbf{r}_i \times (\sum_{j=1}^{N}\mathbf{r}_j \times \mathbf{F}_j). \tag{32}$$

It can be seen from (32) that the force controller of an individual follower robot is highly correlated with other followers, as a result of using local measurements. It is therefore necessary to study the aggregate behavior of all the forces together. Lemma 3 below stacks all the forces into a column force vector and express (32) in a compact matrix form by converting the cross product into matrix multiplication using skew symmetric matrices.

Lemma 3. *The forces of all robots in P-ANTS individually characterized by Eq. (32) can be gathered in one matrix equation,*

$$\dot{\boldsymbol{F}} = \left(-L_a - \frac{M}{J}R_a(t)\right)\boldsymbol{F}, \tag{33}$$

where $\boldsymbol{F} = (f_{1x}, f_{1y}, \cdots, f_{Nx}, f_{Ny})^T$. $L_a = (L_{ij})_{2N\times 2N}$, *where*

$$L_{ij} = \begin{cases} \begin{pmatrix} N-1 & 0 \\ 0 & N-1 \end{pmatrix} & \text{if } i = j \\ \begin{pmatrix} -1 & 0 \\ 0 & -1 \end{pmatrix} & \text{if } i \neq j, \end{cases} \tag{34}$$

and $R_a(t) = (R_{ij}(t))_{2N\times 2N}$, *where*

$$R_{ij}(t) = \begin{pmatrix} -r_{iy}r_{jy} & r_{iy}r_{jx} \\ -r_{ix}r_{jy} & -r_{ix}r_{jx} \end{pmatrix}.$$

The scalar value r_{ix} and r_{iy} denote the x and y component of $\boldsymbol{r}_i$ respectively.

Proof. See the Appendix. □

The expression (33) gives the dynamics of all the robots' forces in the system, and is the main subject of study in this section. The force convergence can be determined by investigating the equilibria and stability of (33). Note that the L_a matrix is just an extension of the graph Laplacian matrix (Olfati-Saber and Murray (2004)). The main challenge is that the matrix $R_a(t)$ is time-varying such that the stability of (33) cannot simply be determined by the locations of the eigenvalues. We deal with the time-varying $R_a(t)$ term by proposing the following two propositions that characterize the time-invariant properties of (33).

Proposition 2. *The rank of $R_a(t)$ is one, and the single nonzero eigenvalue of $R_a(t)$ is a constant $\lambda_{\min}(R_a(t)) = -\sum_{i=1}^{N}\|\boldsymbol{r}_i\|^2$.*

Proof. See the Appendix. □

Proposition 3. *Under the Assumption 3, the eigenvalues of $(-L_a - \frac{M}{J}R_a(t))$ are less than or equal to zero if*

$$\frac{M}{J}\sum_{i=1}^{N}\|\boldsymbol{r}_i\|^2 < N. \tag{35}$$

Furthermore, there are exactly two eigenvalues of value zero with

$$\boldsymbol{1}_x = \begin{pmatrix} 1 \\ 0 \\ 1 \\ 0 \\ \vdots \\ 1 \\ 0 \end{pmatrix}_{2N\times 1}, \quad \boldsymbol{1}_y = \begin{pmatrix} 0 \\ 1 \\ 0 \\ 1 \\ \vdots \\ 0 \\ 1 \end{pmatrix}_{2N\times 1}$$

as the associated eigenvectors.

Proof. First let us look at the eigenvectors associated with the zero eigenvalues. From the properties of the Laplacian matrix we know that $L_a\mathbf{1}_x = L_a\mathbf{1}_y = \mathbf{0}$. Secondly, according to our centrosymmetric assumption, for $\forall i$, $\exists j \neq i$, $s.t.$ $\mathbf{r}_i + \mathbf{r}_j = 0$, or alternatively, $\|\mathbf{r}_i\|\cos(\theta + \theta_i) + \|\mathbf{r}_j\|\cos(\theta + \theta_j) = \mathbf{0}$ and $\|\mathbf{r}_i\|\sin(\theta + \theta_i) + \|\mathbf{r}_j\|\sin(\theta + \theta_j) = \mathbf{0}$. By (42), $R_a(1,:)\mathbf{1}_x = \|\mathbf{r}_1\|\sin(\theta + \theta_1)\sum_{i=1}^{N}\big(-\sin(\theta + \theta_i)\big) = 0$, $R_a(1,:)\mathbf{1}_y = \|\mathbf{r}_1\|\sin(\theta + \theta_1)\sum_{i=1}^{N}\big(\cos(\theta + \theta_i)\big) = 0$. Due to the fact that all rows of $R_a(t)$ are linearly dependent on the first row, we have $(-L_a - \frac{M}{J}R_a(t))\mathbf{1}_x = \mathbf{0}$, $(-L_a - \frac{M}{J}R_a(t))\mathbf{1}_y = \mathbf{0}$.

The eigenvalue of the sum of two matrices can be bounded by Weyl's theorem (Horn and Johnson (2012)), which is a result for Hermitian matrices. L_a is obviously a real symmetric matrix, and therefore it is Hermitian. Since $R_a(t) = (R_{ij}(t))$, and

$$R_{ji}(t) = \|\mathbf{r}_i\|\|\mathbf{r}_j\| \begin{pmatrix} -\sin(\theta+\theta_j)\sin(\theta+\theta_i) & \sin(\theta+\theta_j)\cos(\theta+\theta_i) \\ \cos(\theta+\theta_j)\sin(\theta+\theta_i) & -\cos(\theta+\theta_j)\cos(\theta+\theta_i) \end{pmatrix}.$$

By comparing with (42) we have $R_{ij}(t) = (R_{ji}(t))^T$. This implies that $R_a(t)$ is also a real symmetric (and therefore Hermitian) matrix.

Arrange the eigenvalues of $-L_a$ and $-\frac{M}{J}R_a(t)$ in increasing order,

$$\lambda_1(-L_a^-) \to \lambda_{2N}(-L_a^-):$$
$$-N \leqslant -N \leqslant \cdots \leqslant -N \leqslant 0 \leqslant 0,$$
$$\lambda_1(-\tfrac{M}{J}R_a^-) \to \lambda_{2N}(-\tfrac{M}{J}R_a^-):$$
$$0 \leqslant 0 \leqslant \cdots \leqslant 0 \leqslant \frac{M}{J}\sum_{i=1}^{N}\|\mathbf{r}_i\|^2.$$

If we also arrange the eigenvalues of $-L_a - \frac{M}{J}R_a(t)$ in increasing order, then according to Weyl's,

$$\begin{aligned}\lambda_{2N-2}(-L_a - \frac{M}{J}R_a(t)) &\leqslant \lambda_{2N-2}(-L_a) + \\ &\quad \lambda_{2N}(-\frac{M}{J}R_a(t)) \\ &\leqslant -N + \frac{M}{J}\sum_{i=1}^{N}\|\mathbf{r}_i\|^2.\end{aligned}$$

If $\frac{M}{J}\sum_{i=1}^{N}\|\mathbf{r}_i\|^2 < N$, then

$$\lambda_{2N-2}(-L_a - \frac{M}{J}R_a(t)) < 0,$$

which means that the third largest eigenvalue of $-L_a - \frac{M}{J}R_a(t)$ is less than zero. We also know that $-L_a - \frac{M}{J}R_a(t)$ has two eigenvalues at zero, so $\lambda_{2N-1}(-L_a - \frac{M}{J}R_a(t)) = \lambda_{2N}(-L_a - \frac{M}{J}R_a(t)) = 0$. In summary, $-L_a(t) - \frac{M}{J}R_a(t)$ has two zero eigenvalues with $\mathbf{1}_x$, $\mathbf{1}_y$ as the eigenvectors, and all other eigenvalues are negative. □

Having gathered enough understanding on the time-varying nonlinear force dynamics in P-ANTS, we can now return to our primary goal of showing the convergence of followers' forces to the leader's input force. The first thing we need to do is to separate the leader and the followers in (33). Define $\tilde{L}(t) = (L_a + \frac{M}{J}R_a(t))$. As proposed in Ji et al. (2006), we can separate the leader and followers in $\tilde{L}(t)$ as

$$\tilde{L}(t) = \begin{bmatrix} \tilde{L}_l(t) & \tilde{L}_{fl}^T(t) \\ \tilde{L}_{fl}(t) & \tilde{L}_f(t) \end{bmatrix},$$

where $\tilde{L}_l(t) \in \mathbb{R}^{2\times 2}$, $\tilde{L}_f(t) \in \mathbb{R}^{(2N-2)\times(2N-2)}$ and $\tilde{L}_{fl}(t) \in \mathbb{R}^{(2N-2)\times 2}$. Now we can rewrite (33) in the sense of leader-following:

$$\dot{\mathbf{F}}_f = -\tilde{L}_f(t)\mathbf{F}_f - \tilde{L}_{fl}(t)\mathbf{F}_1, \tag{36}$$

where $\mathbf{F}_f \in \mathbb{R}^{2N-2}$ is the stacked force vector of all follower robots. The objective here is to show that given the leader's input force $\mathbf{F}_1$, every follower robot's force $\mathbf{F}_i$, $i = \{2, 3, \cdots, N\}$, will converge to $\mathbf{F}_1$. This is proved through the following proposition and theorem.

Proposition 4. *$\tilde{L}_f(t)$ has full rank under Assumption 3.*

Proof. From Proposition 3 we know that $\tilde{L}(t)$ has $2N-2$ non-zero eigenvalues, so $rank(\tilde{L}(t)) = 2N-2$, meaning that $\tilde{L}(t)$ has $2N-2$ linearly independent rows (and columns) and 2 linearly dependent rows (and columns). $\tilde{L}_f(t)$ can be obtained by removing the first two rows and columns of $\tilde{L}(t)$. Denote the i-th row and j-th column of $\tilde{L}(t)$ by $\tilde{L}(i,:)$ and $\tilde{L}(:,j)$. Then by (34), (42), (43), (44) we have $\tilde{L}(1,:) = -(\tilde{L}(3,:) + \tilde{L}(5,:) + \cdots + \tilde{L}(2N-1,:))$, $\tilde{L}(2,:) = -(\tilde{L}(4,:) + \tilde{L}(6,:) + \cdots + \tilde{L}(2N,:))$, $\tilde{L}(:,1) = -(\tilde{L}(:,3) + \tilde{L}(:,5) + \cdots + \tilde{L}(:,2N-1))$, $\tilde{L}(:,2) = -(\tilde{L}(:,4) + \tilde{L}(:,6) + \cdots + \tilde{L}(:,2N))$. In other words, the first two rows (columns) of $\tilde{L}(t)$ are linearly independent of each other, but linearly dependent on the other rows (columns) of $\tilde{L}(t)$. Therefore, after removing these two rows and columns, $\tilde{L}_f(t)$ still has $2N-2$ linearly independent rows (columns), and hence it has full rank. □

The following Lemma will be important in proving the convergence of the follower forces to the leader's force.

Lemma 4. ***(Cauchy's interlacing theorem** (Horn and Johnson (2012)) Let B be a submatrix of $A = \begin{bmatrix} B & y \\ y^T & a \end{bmatrix}$, where B is a Hermitian matrix in $\mathbb{R}^{N\times N}$, $A \in \mathbb{R}^{(N+1)\times(N+1)}$, $y \in \mathbb{R}^N$ and $a \in \mathbb{R}$. Then*

$$\begin{aligned}\lambda_1(A) \leqslant \lambda_1(B) \leqslant \lambda_2(A) \leqslant \cdots\cdots \\ \leqslant \lambda_N(A) \leqslant \lambda_N(B) \leqslant \lambda_{N+1}(A).\end{aligned}$$

Theorem 7. *(P-ANTS Local) Under the centrosymmetric assumption (Assumption 3) and the geometric condition (35), all followers' forces in (36) will converge asymptotically to the leader's force $\boldsymbol{F}_1$.*

Proof. We first show that all the eigenvalues of $-\tilde{L}_f(t)$ are negative. By removing the first two rows and columns of

$-\tilde{L}(t)$, we can apply Lemma 4 twice and get

$$\lambda_1(-\tilde{L}(t)) \leqslant \lambda_1(-\tilde{L}_f(t)) \leqslant \cdots\cdots \leqslant \lambda_{2N-2}(-\tilde{L}_f(t)) \leqslant \lambda_{2N-1}(-\tilde{L}(t)) = 0.$$

By Proposition 4, $\tilde{L}_f(t)$ has full rank, so $\tilde{L}_f(t)z = 0$ has no nonzero solution. Thus we know $\lambda_{2N-2}(-\tilde{L}_f(t)) < \lambda_{2N-1}(-\tilde{L}(t)) = 0$, that is, the largest eigenvalue of $\tilde{L}_f(t)$ is strictly less than zero.

Looking at (36), one can see that $\mathbf{F}_f^{eq} = [\mathbf{F}_1, \mathbf{F}_1, \cdots, \mathbf{F}_1]^T$ is an invariant equilibrium point, although the system is time-varying. Furthermore, since $\tilde{L}_f(t)$ has full rank, $\dot{\mathbf{F}}_f = -\tilde{L}_f(t)\mathbf{F}_f - \tilde{L}_{fl}(t)\mathbf{F}_1 = \mathbf{0}$ has an unique solution, such that $\mathbf{F}_f^{eq}$ is the only equilibrium point. Then we can decompose $\mathbf{F}_f$ as

$$\mathbf{F}_f = \mathbf{F}_f^{eq} + \boldsymbol{\delta}. \tag{37}$$

The dynamics of the disagreement vector $\boldsymbol{\delta}$ can be obtained by

$$\begin{aligned}\dot{\mathbf{F}}_f = \dot{\boldsymbol{\delta}} &= (-\tilde{L}_f(t))(\mathbf{F}_f^{eq} + \boldsymbol{\delta}) + \tilde{L}_{fl}(t)\mathbf{F}_1 \\ &= -\tilde{L}_f(t)\boldsymbol{\delta} + (-\tilde{L}_f(t)\mathbf{F}_f^{eq} + \tilde{L}_{fl}(t)\mathbf{F}_1) = -\tilde{L}_f(t)\boldsymbol{\delta}.\end{aligned}$$

Choose the Lyapunov function

$$V = \frac{1}{2}\boldsymbol{\delta}^T\boldsymbol{\delta},$$

we have

$$\dot{V} = \boldsymbol{\delta}^T\dot{\boldsymbol{\delta}} = \boldsymbol{\delta}^T(-\tilde{L}_f(t))\boldsymbol{\delta} \leqslant \lambda_{2N-2}(-\tilde{L}_f(t))\|\boldsymbol{\delta}\|^2 < 0.$$

Then by the Lyapunov theorem, we have $\boldsymbol{\delta} \to \mathbf{0}$. Since the disagreement $\boldsymbol{\delta}$ will vanish to zero asymptotically, we know by (37) that all followers' forces will converge to the leader's force asymptotically. □

The result of Theorem 7 shows that P-ANTS is still effective even when the follower robots use local measurements (5), (6) under a centrosymmetric Assumption 3 and a mild geometric condition (35). Since every follower's force will converge to the leader's force in the steady state, the steady state gain of the output force to the input force will be N.

6. Simulations

Simulations are done for both CB-ANTS and P-ANTS with local measurements to verify Theorem 3 and Theorem 7. We conduct our simulations in Open Dynamics Engine (ODE), a well-known physics engine in the robotics community. With the help of the simulator, we can focus only on the behavior of the robots and let the simulator account for all the forces, torques and planar rigid-body object dynamics.

6.1. CB-ANTS Simulation

As mentioned in the Introduction section, CB-ANTS is suitable for the scenario where the scale of the object is moderate and the required number of robots is relatively small. We choose the object to be a small chair that weighs 2kg and its dimensions are: length 0.6m, width 0.4m and height 0.8m. We manipulate the chair with a group of 20 robots. Each of the followers can apply a force up to 0.8N while the leader has a bit larger capacity, up to 0.96N. The coefficient μ_k is set to be 0.59 and the acceleration of the gravity $g = 9.8m/s^2$. An easy calculation yields that at least 15 robots are required to overcome the kinetic friction. The simulated robots have noisy sensing and actuation. The measured velocities of the object, at robots' local attachment points, are corrupted by zero-mean Gaussian noise $\mathcal{N}(0, 0.01I_2)$, where I_2 is a two-dimensional identity matrix. We also assume that the robots cannot apply absolutely accurate forces, so another Gaussian noise $\mathcal{N}(0, 0.05I_2)$ is added to the desired forces of the follower robots calculated by (7). The robots are arranged in a centrosymmetric configuration along the bottom of the chair, as shown in Figure 7. For simplicity, we do not draw any specific grasping mechanism and abstract the robots as spheres instead. The goal is to navigate the chair through a specific trajectory while avoiding all the obstacles. In order to achieve this, we find several pre-defined waypoints and specify the leader's controller (8) using a simple strategy as follows: let $\mathbf{v}_d$ always point from the object's center of the mass towards the next unreached waypoint with a constant magnitude at $0.3m/s$. Small circular regions around the waypoints are also defined to mark the arrival of the object. Once the object hits the circular region, the leader then switches to the next waypoint. There may be better waypoint following algorithms, but that is not the focus of this paper, and we find that the simple strategy is good enough to navigate the object through waypoints one by one. In order to limit the angular velocity and satisfy condition (19), we let the leader's torque input be $\mathbf{T}_1 = -0.1\boldsymbol{\omega}$.

Figure 8 shows that the robots successfully follow the waypoints and transport the chair to the destination. Figure 9 shows the forces of both the leader and follower robots during the simulation. Although the forces applied by different follower robots are slightly different due to the heterogeneous local measurements, the force convergence, as proven in Theorem 3, is evident in Figure 9 even when the leader's force is changing. The visualization of the bound condition (19) is shown in Figure 10. When the angular velocity stays strictly within the bound, the forces converge quickly and the linear velocity of the object can be steadily maintained at the desired $0.3m/s$. Violation of the bound is allowed, since the object keeps moving all the time and as explained in Remark 1 after Theorem 3, however,

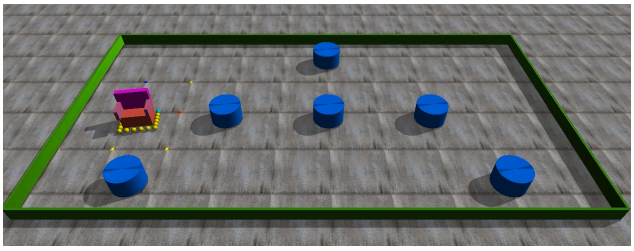

Figure 7. Simulation setup in ODE. The chair is in red. 20 robots, denoted by spheres, surround the chair at the bottom. The yellow spheres are follower robots while the leader is in light blue, situated at the upper right conner of the chair. The blue cylinders are obstacles that should be avoided by the object.

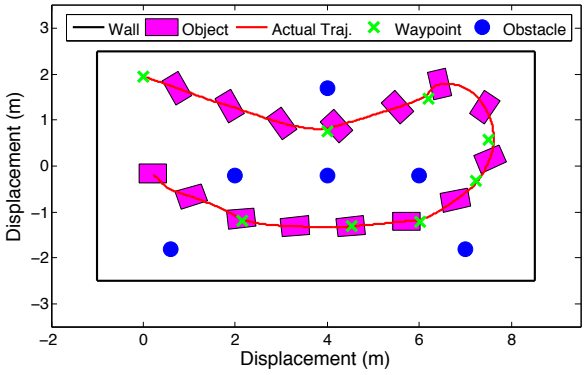

Figure 8. The trajectory of the object in the simulation. The object is drawn every 4 seconds.

the magnitude of the linear velocity may drop due to the increased disturbance, as is the case when t is between $30s$ and $38s$ in Figure 10.

6.2. P-ANTS Simulation

Compared to CB-ANTS, P-ANTS is good at handling objects of a large scale with a large number of robots. Therefore, we choose the simulated object to be a grand piano that has the same dimensions as a realistic Steinway K-52 piano: weight 273kg, length 1.54m, width 0.67m, height 1.32m. We have a group of 1000 robots, each of which can apply a force up to 0.3N. The parameters of the environment are set to be $\mu_v = 0.3$ and $g = 9.8m/s^2$. As in the CB-ANTS case, we simulate the noisy sensing and actuation of the robots by adding zero-mean Gaussian noise, i.e., $\mathcal{N}(0, 0.03I_2)$ for local velocity measurements, $\mathcal{N}(0, 0.05I_2)$ for local acceleration measurements, and $\mathcal{N}(0, 0.1I_2)$ for force actuation.

We have a more ambitious goal in this simulation compared to the previous one: navigate the object through a narrow maze. In order to achieve this more precise trajectory following, we design the leader's control strategy

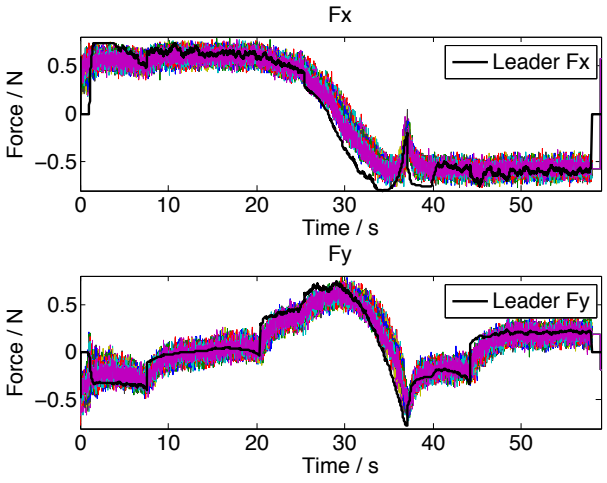

Figure 9. Forces of the robots during the simulation. The bold black line is the desired input force of the leader robot. Other colored lines are the forces of the followers, which are very noisy due to the noisy sensing and actuation. The abrupt jumps of the leader's force are due to the switching between old and new waypoints.

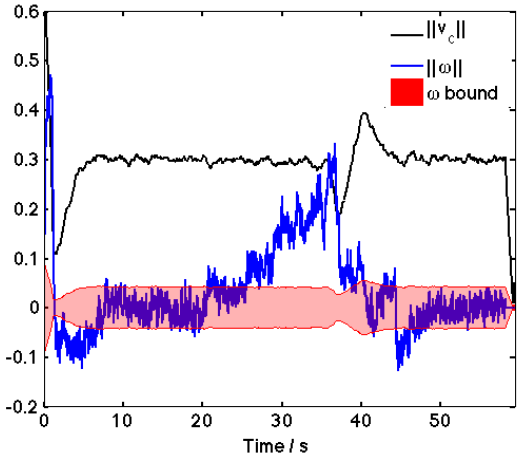

Figure 10. The magnitude of the linear and angular velocity of the object during the CB-ANTS simulation are drawn in black and blue line. This figure reveals that the bound condition (19), denoted by the red region, is conservative. Even when the angular velocity violates the bound, the object keeps moving. However, the penalty is that the linear velocity drops due to the disturbance from local velocity measurements.

as follows. First, find the point on the desired trajectory that is nearest to the objects current position, defined as x_a. Also, define the current position of the object as x_c. Then the desired velocity can be defined as $\mathbf{v}_d = w_n\mathbf{v}_n + w_t\mathbf{v}_t$, as shown in Figure 11, where $\mathbf{v}_n = \frac{x_a - x_c}{\|x_a - x_c\|}$ is the unit normal vector, $\mathbf{v}_t$ is the unit tangential vector at x_a pointing to the destination and w_n, w_t are weights. Intuitively, $\mathbf{v}_n$ will drag the object towards the trajectory and $\mathbf{v}_t$

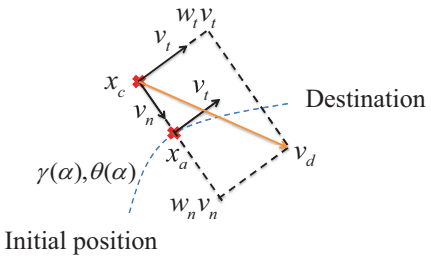

Figure 11. The synthesis of the desired linear velocity v_d.

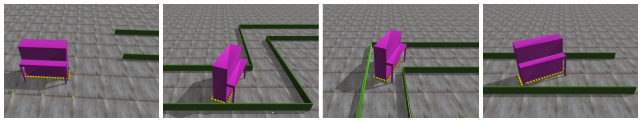

Figure 12. Manipulation of a large simulated Steinway K-52 piano (purple) with 1000 robots. Robots are centrosymmetrically distributed around the bottom of the piano. For visualization considerations, we draw 40 robots instead of 1000. The width of the maze varies from 1.4m to 2m.

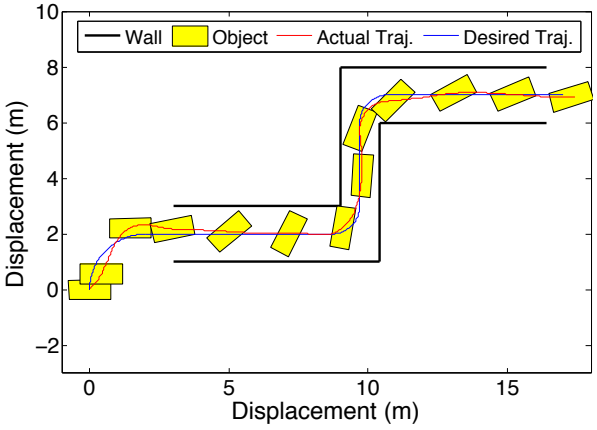

Figure 13. Overall trajectory of the piano. The piano is drawn every 8 seconds.

will maintain the object's velocity along the trajectory. Secondly, the leader robot can implement a force feedback controller $\mathbf{F}_1 = K_f(\mathbf{v}_d - \mathbf{v})$ that can drive the object's velocity to the desired velocity. Furthermore, the orientation of the object can be controlled by the leader's direct torque input as introduced in Section 3.4. The maximal capability of the leader's torque input is set to be $50Nm$.

The snapshots of the piano moving experiment are shown in Figure 12. The entire trajectory of the piano is shown in Figure 13. It can be seen that the piano can be successfully transported through the narrow maze.

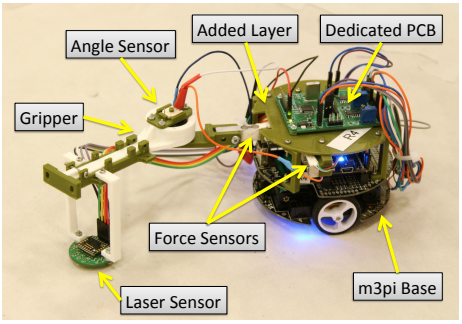

Figure 14. Our custom-built manipulation robot with key components shown.

7. Robot Design

We build a robot prototype to verify CB-ANTS experimentally. Our design brings together a series of sensing, computation and actuation capabilities in order to verify our theory experimentally. We insist on keeping our robot as simple and low-cost as possible. Therefore, we build our robot upon a commercially available, affordable robot called the m3pi from Pololu,[†] as shown in Figure 14. The m3pi robot uses a differential drive scheme, and is controlled by an mbed-enabled[‡] LPC1768 micro-controller running at 96MHz. We integrate more functionality into the m3pi robot, through customized hardware and software components described below.

7.1. Mechanical Design

The original m3pi robot comes with two layers. The base layer contains batteries, motors and related driving circuits. The second layer hosts the LPC1768 micro-controller. We add an additional third layer to accommodate our force sensors (Figure 16) and customized PCB. Besides the robot, we also build a gripper (Figure 15) that consists of one revolute joint, realized through a bearing and a shaft. The gripper can be mounted to the robot on the tip of the force sensor through screws. The other side of the gripper can be manually attached to the object, also using screws. Mounting holes for holding the optical sensor are available on the object side of the gripper. All the customized mechanical components are 3D-printed.

7.2. Force Sensing

Each robot is equipped with a force sensing unit (Figure 16), consisting of two load cells that are installed perpendicularly in order to measure the 2D force applied by the robot to the object in the x and y direction.

[†] www.pololu.com
[‡] mbed.org

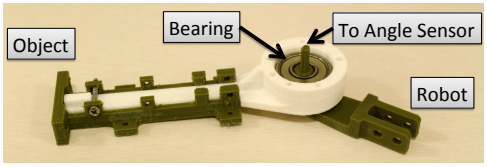

Figure 15. The one DOF gripper. The long shaft is connected to the rotary potentiometer to obtain the angle reading.

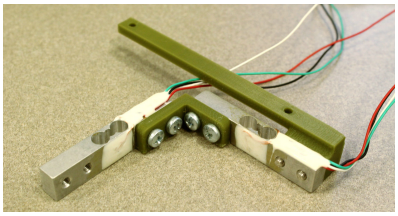

Figure 16. The force sensing unit, consisting of two perpendicularly connected load cells.

Each load cell, having four strain gauges configured as a Wheatstone bridge, can measure the force in one direction. The differential output voltages are amplified and measured on a dedicated PCB, which has an STM32 micro-controller running at 72MHz. STM32 can then send the A/D data to our main controller LPC1768 via serial port. Before usage, each load cell is carefully calibrated using multiple calibration weights. The capacity of each load cell is -2N to 2N.

7.3. Velocity Sensing

We measure the velocity of the object using an ADNS9800 optical laser sensor, typically used in the optical mouse. The sensor outputs the delta distance in x and y direction to the LPC1768 via Serial Peripheral Interface (SPI) bus. We then differentiate the distance signal with the time interval to get the average velocity. The laser sensor is installed as close as possible to the object on the gripper in order to minimize the disturbance caused the by the heterogenous local measurements. Two holders extending from the gripper make sure that the optical sensor touches the ground properly.

7.4. Angle Sensing and Miscellaneous

Since the robot and the object do not necessarily have the same heading, the angle measurement on the revolute joint of the gripper is needed in order to convert velocity from the object's reference frame to the robot's frame. We place a rotary potentiometer on top of the rovolute joint, and connect it with the shaft via the through-hole on the sensor. The voltage is then sampled by LPC1768 and converted into an angle value.

There is no global localization information for the follower robots. However, we track the position of the leader robot through an OptiTrack[§] system by placing reflective markers on the leader (Figure 6). This matches our assumption that only the leader robot knows the destination. Note that there is an Xbee wireless module on each robot, but the follower robot does not use it for any kind of communication during the experiment. The follower robots only use Xbee to receive a start command before the experiment and upload their sensor measurement histories to a computer for analysis after the experiment.

7.5. Force Feedback Control

In order to implement the controller (7), (8), robots first need to be able to control how much force they apply along the x and y directions. We can generate the force by controlling the two wheel speeds of our robot. Here we introduce our low-level force feedback controller that maps the force generation to motor control.

Our force feedback controller contains three steps. First of all, since the velocity measured by the laser sensor (attached rigidly to the object) is in the object's frame, we need to convert it into the robot's local frame. This is achieved by

$$\mathbf{v}^i = R(\theta_i)\mathbf{v}, \tag{38}$$

where i specifies the robot, θ_i is angle sensor reading of the joint on the gripper and $R(\cdot)$ represents the rotation matrix.

The second step is force generation. Briefly speaking, the forces come from the robots' tendencies to go faster or slower than the object. The larger the tendency is, the greater the force will be and vice versa. Alonso-Mora et al. (2015) characterize this tendency by the difference between the commanded velocity of the robot and the actual velocity of the object. Thus, we can use a linear model to describe this phenomenon, given by

$$\mathbf{v}_c^i - \mathbf{v}^i = K_f(\mathbf{F}_i - \mathbf{f}_i), \tag{39}$$

where $\mathbf{v}_c^i$ represents the commanded velocity of robot i, $\mathbf{F}_i$ is the desired force in (7) and $\mathbf{f}_i$ is the actual force vector applied by robot i measured by force sensors. The parameter K_f is a constant that needs to be tuned experimentally.

The last step is to fulfill the commanded velocity $\mathbf{v}_c^i$ on the robot. Note that although our differential-driven robot is non-holonomic, Michael and Kumar (2009) show that an offset point outside the center of the mass of the robot can be holonomic. Since the joint on the gripper is where the force is measured and applied, we choose the pivot of the joint to be our holonomic offset point. Denote the angular

[§] http://www.optitrack.com

velocity of the left and right motor as ω_l and ω_r, the radius of the wheels as r_w, the distance between two wheels as d_w, and the offset distance of the point from the center of the mass as l. Then the velocity of the offset point can be written as

$$\mathbf{v}_p^i = \left[\frac{(\omega_l - \omega_r)r_w l}{d_w}, \frac{(\omega_l + \omega_r)r_w}{2}\right]. \quad (40)$$

Letting $\mathbf{v}_p^i = \mathbf{v}_c^i$, we can solve for the wheel speeds and then output the command to the two motors respectively.

8. Experiments

The effectiveness of CB-ANTS is successfully verified through experiments, while the physical experiment for P-ANTS is left for future work. We build four robots to manipulate a cardboard box, whose weight is 270g. The friction is approximately 1.6N, so μ is equal to 0.59. Each robot is able to apply a maximum force at about 0.8N on its own. Note that the friction coefficient and force limit of the robots are the same as they are in the simulation. The experiment is conducted in a 4m $\times$ 2.5m arena, which is covered by an Optitrack motion capture system. Only the leader and the object are tracked by Optitrack. In all experiments, we skip the initial random force trials as described in Section 3.2 since this is not the focus of the paper. Instead, we send one kickoff command via XBee assigning robots an initial speed. The robots are initially placed in the same direction along the width of the box, and all the robots are given the same initial forward speed (in the box's frame) to generate an aligned initial force to move the object. After that and during the experiments, the follower robots complete all the sensing and computation onboard, without having access to communication and localization information. We conducted three experiments with three different types of leaders (either a robot or human), while the followers are the same for all trials. All the experiments are run multiple times (80 times for Section 8.1, 80 times for Section 8.2, and 20 times for Section 8.3) to ensure repeatability.

8.1. Leader is an Autonomous Robot

In this case, the leader robot pulls the front of the object while three follower robots push on the side or back. Note that the configuration of the robots is not unique since our algorithm only cares about the forces rather than the positions of the robots. Three follower robots are also interchangeable because they have the same hardware and run the same program. The leader robot receives commands wirelessly via XBee from a computer, where controller (8) is implemented. In contrast to the follower robots, which have local sensing and control onboard, the leader robot has external sensing from Optitrack and does not have onboard angle and velocity sensor.

The task setup is the same as the simulation. Figure 17 shows the snapshots of the waypoint following process. The outcome trajectory demonstrates various coordinated actions of the group, such as line tracking, left and right turns, and a U-turn. This indicated that our robotic fleet is able to execute trajectories other than the one demonstrated here. The force, velocity, and angle measurements of the robots are recorded at 10Hz and then uploaded for analysis after the manipulation is done. Figure 18 plots the force histories of the robots. From Figure 18(a) we can see that the magnitudes of followers' forces are close to the desired 0.4N, and the leader's force is slightly larger than the followers', matching our analysis in Remark 1 of Theorem 1 and Remark 3 of Theorem 3. In Figure 18(b)–(d), we plot the followers' force records in a rotated local reference frame, where the y axis is the direction of $\mathrm{v}_i(t)$ at every sampling time. Ideally, the follower's force should be located at (0,0.4) according to (7). Due to noise and disturbances in the system, the forces scatter around the y axis. However, the average forces are close to the desired force at (0,0.4) and nearly all the force samples have positive y component, indicating that the follower robots actively help the leader in the process rather than dragging behind.

8.2. Leader is a Robot Tele-operated by Human

We show human-swarm cooperation in the next two manipulation experiments. One advantage of our algorithm is that the follower robots will synchronize to the leader's force, no matter where the force is from. This allows the robotic swarm to interact and cooperate with a human leader. In this experiment, we keep all the settings for the three follower robots, and manually control the leader robot using a remote joystick instead of running the automatic waypoint following program. The joystick, as shown in Figure 19, captures the wheel speeds specified by a human operator in real time and then sends the commands to the leader robot via XBee. For the convenience of comparison, we keep the destination and obstacles the same as before. As shown in the video, the follower robots can successfully cooperate with the human operator to transport the object. To check the effectiveness of this human-swarm cooperation, we plot the forces of all the robots as before in Figure 20. It can be seen that all the follower robots contribute positive forces most of the time, although there do exist some negative ones compared to Figure 18. The negative forces of the follower robots are caused by the abrupt hard pulling of the leader robot due to the lack of force feedback for the human operator.

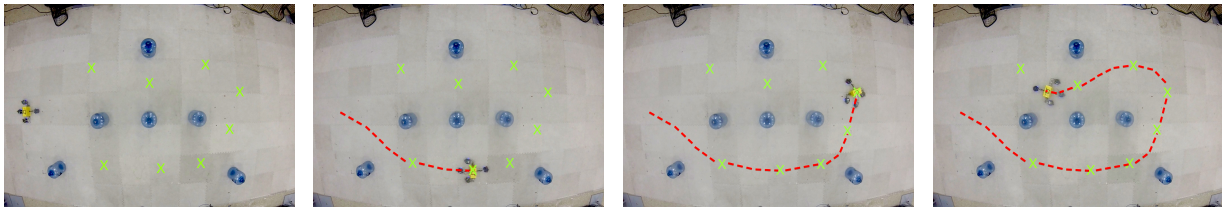

(a) $t = 0$ (b) $t = 26$s (c) $t = 45$s (d) $t = 62$s

Figure 17. Snapshots of the waypoint following process. Green "X"s are waypoints and the red dotted line is the actual trajectory.

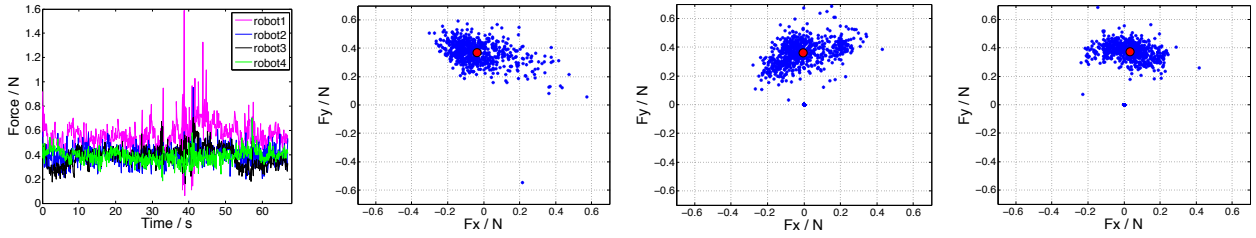

(a) Force magnitude (b) Robot 2 (c) Robot 3 (d) Robot 4

Figure 18. Forces measured during *Experiment 8.1*. (a): The magnitude of the forces applied by all the robots. (b)-(d): The force histories applied by robot 2, 3 and 4, respectively in each robot's local frame, and the red dot denotes the average force. Ideally, followers' forces should be located in (0, 0.4). The figures verify that the all the follower robots contribute positive forces to the object during the experiment.

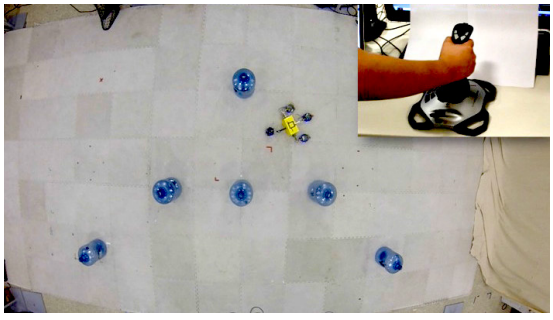

Figure 19. Leader robot is controlled by a human operator via a remote joystick in *Experiment 8.2* . The human operator uses visual feedback to control the leader robot, without knowing the state and sensor readings of the follower robots. The follower robots run the same program as in the previous experiment 8.1, without knowing the command sent by the human to the leader robot.

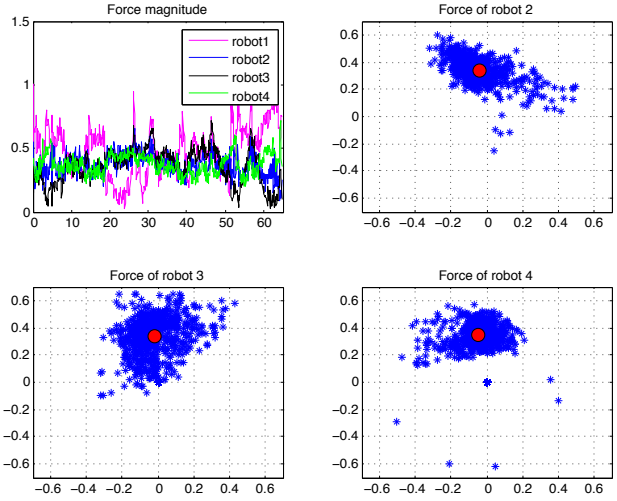

Figure 20. Force plots of *Experiment 8.2* . The way we plot them is the same as Figure 18. The data here present resemblance to the previous autonomous robot leader case, validating the followers' successful cooperation with the human leader in this experiment.

8.3. Leader is a Human

To further interact with the robots more directly, we let a human grasp the object instead of tele-operating a leader robot. As shown in Figure 21, the human leader gently holds the gripper and guides the follower robots. The human leader tries to apply a small force to the object within the same scale as the robots, in order to prevent overwhelming the robots' forces. Although we have not yet developed a device to measure the force from the hand of the human leader, the contribution of the follower robots can be verified through the force plotting again in Figure 22. The forces are more scattered than the previous

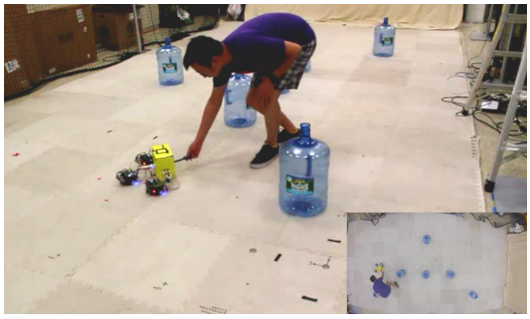

Figure 21. Three follower robots cooperate with a human leader.

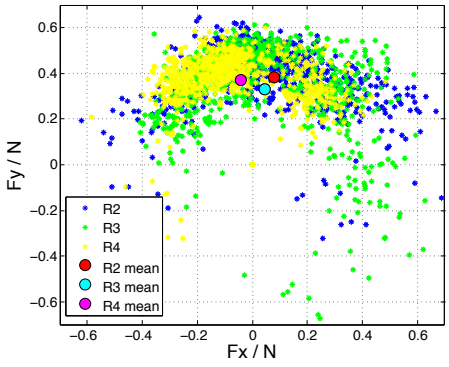

Figure 22. Forces of three follower robots in *Experiment 8.3* . In the interest of space we have shown them all on the same plot. Although followers' forces are more scattered in this case, the mean forces reflect their positive contribution and successful cooperation with the human leader.

two experiments, because it is relatively more difficult for the human leader to maintain a constant, small force in this case. However, the followers' mean forces still stay around the ideal $(0, 0.4)$.

9. Conclusion and Future Work

In this paper, we propose the framework of a Multi-Robot Force-Amplifying System that coordinates the manipulation forces from a group of robots in order to collectively transport a heavy object. The leader's guiding force can be amplified by many follower robots, which synchronize their forces to the leader's force by locally measuring the motion of the object at their attachment points. This framework characterizes a class of fully distributed and scalable controllers that achieve force coordination without explicit communication among robots. We propose two specific controller implementations within the framework to deal with two different scenarios of the manipulation task. The first implementation, CB-ANTS handles the nonlinear kinetic friction well and provides a constant boost force by the followers. The second implementation, P-ANTS takes advantage of the linear dynamics of the object due to the linear viscous friction, and enables the leader to steer both the direction and magnitude of the group force. Our approach can successfully handle the heterogeneous local motion measurements, requiring only a bound on the angular velocity (19) or a mild geometric condition (35), which are practical and achievable in real applications. We also quantitatively show why a centrosymmetric placement of the robots is beneficial to the performance of the multi-robot manipulation, as in Theorem 4 and throughout the proofs in Sec. 5.4. Simulations are done to verify both CB-ANTS and P-ANTS with up to 1000 robots. Four proof-of-concept robots are built to experimentally validate CB-ANTS. We also successfully demonstrate the human-swarm cooperative manipulation by two experiments.

In the future, there are many directions in which we can extend our approach. We can use adaptive control or machine learning to estimate the key parameters the robots need to know in Assumption 1. Under our Force-ANTS framework, there are many possibilities for more adaptive and intelligent controllers to be explored in the future. We plan to work on decentralized rotation control with the efforts from all the robots and still without communication. On the hardware side, we plan to use the omnidirectional robot platform, which is not limited by the non-holonomic constraint and can therefore achieve more accurate 2D force feedback control with better mobility. Ultimately, we want to experiment in transporting meaningful objects of realistic sizes.

Acknowledgements

This work was supported in part by NSF grant CNS-1330036. The authors are grateful for the support.

References

Wang Z and Schwager M (2014) Multi-Robot Manipulation Without Communication. *International Symposium on Distributed Autonomous Robotic Systems (DARS)*, pp. 135–149.

Wang Z and Schwager M (2016) Kinematic Multi-Robot Manipulation with no Communication Using Force Feedback. In *Proceedings of the IEEE International Conference on Robotics and Automation (ICRA)*, pp. 427–432.

Khatib O (1987) A unified approach for motion and force control of robot manipulators: The operational space formulation. *IEEE Journal of Robotics and Automation*, vol. 3(1), pp. 43–53.

Rus D, Donald B and Jennings J (1995) Moving furniture with teams of autonomous robots. In *Proceedings of the International Conference on Intelligent Robots and Systems (IROS)*, vol. 1, pp. 235–242.

Böhringer Karl, Brown R, Donald B, Jennings J and Rus D (1997) Distributed robotic manipulation: Experiments in minimalism. *Experimental robotics IV*, pp. 11–25.

Donald BR and Jennings J and Rus D (1997) Information invariants for distributed manipulation. *The International Journal of Robotics Research*, vol. 16(5), pp. 673–702.

Song P and Kumar V (2002) A potential field based approach to multi-robot manipulation. In *Proceedings of the IEEE International Conference on Robotics and Automation (ICRA)*, vol. 2, pp. 1217–1222.

Wang ZD and Kumar V (2002) Object closure and manipulation by multiple cooperating mobile robots. In *Proceedings of the IEEE International Conference on Robotics and Automation (ICRA)*, vol. 1, pp. 394–399.

Pereira GA, Campos MF and Kumar V (2004) Decentralized algorithms for multi-robot manipulation via caging. *The International Journal of Robotics Research*, vol. 23(7-8), pp. 783–795.

Wan W, Fukui R, Shimosaka M, Sato T and Kuniyoshi Y (2012) Cooperative manipulation with least number of robots via robust caging. In *Proceedings of the IIEEE/ASME International Conference on Advanced Intelligent Mechatronics (AIM)*, pp. 896–903.

Fink J, Hsieh MA and Kumar V (2008) Multi-robot manipulation via caging in environments with obstacles. In *Proceedings of the IEEE International Conference on Robotics and Automation (ICRA)*, pp. 1471–1476.

Esposito JM (2009) Decentralized cooperative manipulation with a swarm of mobile robots. In *Proceedings of the International Conference on Intelligent Robots and Systems (IROS)*, pp. 5333–5338.

Kennedy MD, Guerrero L and Kumar V (2015) Decentralized algorithm for force distribution with applications to cooperative transport. In *ASME International Design Engineering Technical Conferences and Computers and Information in Engineering Conference*.

Erhart S, Sieber D and Hirche S (2013) An impedance-based control architecture for multi-robot cooperative dual-arm mobile manipulation. In *Proceedings of the International Conference on Intelligent Robots and Systems (IROS)*, pp. 315–322.

Franchi A, Petitti A and Rizzo A (2015) Decentralized parameter estimation and observation for cooperative mobile manipulation of an unknown load using noisy measurements. In *Proceedings of the IEEE International Conference on Robotics and Automation (ICRA)*, pp. 5517–5522.

Williams D and Khatib O (1993) The virtual linkage: A model for internal forces in multi-grasp manipulation. In *Proceedings of the IEEE International Conference on Robotics and Automation (ICRA)*, pp. 1025–1030.

Khatib O, Yokoi K, Brock O, Chang K and Casal A (1999) Robots in human environments: Basic autonomous capabilities. *The International Journal of Robotics Research*, vol. 18(7), pp. 684–696.

Becker A, Habibi G, Werfel J, Rubenstein M and McLurkin J (2013) Massive uniform manipulation: Controlling large populations of simple robots with a common input signal. In *Proceedings of the International Conference on Intelligent Robots and Systems (IROS)*, pp. 520–527.

Rubenstein M, Cabrera A, Werfel Justin, Habibi G, McLurkin J and Nagpal R (2013) Collective transport of complex objects by simple robots: theory and experiments. In *Proceedings of International Conference on Autonomous Agents and Multi-agent Systems (AAMAS)*, pp. 47–54.

Habibi G, Kingston Z, Xie W, Jellins M and McLurkin J (2015) Distributed Centroid Estimation and Motion Controllers for Collective Transport by Multi-Robot Systems. In *Proceedings of the IEEE International Conference on Robotics and Automation (ICRA)*, pp. 1282–1288.

Habibi G, Kingston Z, Wang Z, Schwager M and McLurkin J (2015) Pipelined Consensus for Global State Estimation in Multi-Agent Systems. In *Proceedings of International Conference on Autonomous Agents and Multi-agent Systems (AAMAS)*, pp. 1315–1323.

Amanatiadis A, Henschel C, Birkicht B, Andel B, Charalampous K, Kostavelis I, May R, and Gasteratos A (2015) AVERT: An Autonomous Multi-Robot System for Vehicle Extraction and Transportation. In *Proceedings of the IEEE International Conference on Robotics and Automation (ICRA)*, pp. 1662–1669.

Alonso-Mora J, Knepper R, Siegwart R and Rus D (2015) Local motion planning for collaborative multi-robot manipulation of deformable objects. In *Proceedings of the IEEE International Conference on Robotics and Automation (ICRA)*, pp. 5495–5502.

Donald B, Gariepy L, and Rus D (2000) Distributed manipulation of multiple objects using ropes. In *Proceedings of the IEEE International Conference on Robotics and Automation (ICRA)*, vol. 1, pp. 450–457.

Fink J, Michael N, Kim S and Kumar V (2011) Planning and control for cooperative manipulation and transportation with aerial robots. *The International Journal of Robotics Research*, vol. 30(3), pp. 324–334.

Chen J, Gauci M and Groß R (2013) A strategy for transporting tall objects with a swarm of miniature mobile robots. In *Proceedings of the IEEE International Conference on Robotics and Automation (ICRA)*, pp. 863–869.

Baldassarre G, Trianni V, Bonani M, Mondada F, Dorigo M and Nolfi S (2007) Self-organized coordinated motion in groups of physically connected robots. *IEEE Transactions on Systems, Man, and Cybernetics, Part B: Cybernetics*, vol. 37(1), pp. 224–239.

Hirata Y, Ojima Y and Kosuge K (2008) Variable motion characteristics control of an object by multiple passive mobile

robots in cooperation with a human. In *Proceedings of the IEEE International Conference on Robotics and Automation (ICRA)*, pp. 1346–1351.

Olfati-Saber R and Murray RM (2004) Consensus problems in networks of agents with switching topology and time-delays. *IEEE Transactions on Automatic Control*, vol. 49(9), pp. 1520–1533.

Jadbabaie A, Lin J and Morse AS (2003) Coordination of groups of mobile autonomous agents using nearest neighbor rules. *IEEE Transactions on Automatic Control*, vol. 48(6), pp. 988–1001.

Hong Y, Hu J and Gao L (2006) Tracking control for multi-agent consensus with an active leader and variable topology. *Automatica*, vol. 42(7), pp. 1177–1182.

Tanner HG (2004) On the controllability of nearest neighbor interconnections. In *Proceedings of the IEEE International Conference on Decision and Control (CDC)*, vol. 3, pp. 2467–2472.

Zhang Y and Tian YP (2010) Consensus of data-sampled multi-agent systems with random communication delay and packet loss. *IEEE Transactions on Automatic Control*, vol. 55(4), pp. 939–943.

Li T and Zhang JF (2010) Consensus conditions of multi-agent systems with time-varying topologies and stochastic communication noises. *IEEE Transactions on Automatic Control*, vol. 55(9), pp. 2043–2057.

McCreery HF and Breed MD (2014) Cooperative transport in ants: a review of proximate mechanisms. *Insectes Sociaux*, vol. 61(2), pp. 99–110.

Berman S, Lindsey Q, Sakar MS, Kumar V and Pratt S (2010) Study of group food retrieval by ants as a model for multi-robot collective transport strategies. *Robotics: Science and Systems (RSS)*, pp. 259 – 266.

Wilson S, Pavlic TP, Kumar GP, Buffin A, Pratt SC and Berman S (2014) Design of ant-inspired stochastic control policies for collective transport by robotic swarms. *Swarm Intelligence*, vol. 8(4), pp. 303–327.

Gelblum A, Pinkoviezky I, Fonio E, Ghosh A, Gov N and Feinerman O (2015) Ant groups optimally amplify the effect of transiently informed individuals. *Nature communications*, vol. 6.

Michael N and Kumar V (2009) Planning and control of ensembles of robots with non-holonomic constraints. *The International Journal of Robotics Research*, vol. 28(8), pp. 962–975.

Horn RA and Johnson CR (2012) *Matrix analysis*. Cambridge University Press, pp. 181.

Wang Z and Schwager M (2015) Multi-Robot Manipulation with no Communication Using Only Local Measurements. In *Proceedings of the IEEE International Conference on Decision and Control (CDC)*, pp. 380–385.

Ji M, Muhammad A and Egerstedt M (2006) Leader-based multi-agent coordination: Controllability and optimal control. In *American Control Conference*, pp. 1358–1363.

Stilwell DJ and Bay JS (1993) Toward the development of a material transport system using swarms of ant-like robots. In *Proceedings of the IEEE International Conference on Robotics and Automation (ICRA)*, pp. 766–771.

Kosuge K and Oosumi T (1996) Decentralized control of multiple robots handling an object. In *Proceedings of the International Conference on Intelligent Robots and Systems (IROS)*, vol. 1, pp. 318–323.

Chen J, Gauci M, Li W, Kolling A and Groß R (2015) Occlusion-based cooperative transport with a swarm of miniature mobile robots. In *IEEE Transactions on Robotics*, vol. 31, no. 2, pp. 307–321.

Groß R and Dorigo M (2004) Group transport of an object to a target that only some group members may sense. In *International Conference on Parallel Problem Solving from Nature*, pp. 852–861.

Groß R, Mondada F and Dorigo M (2006) Transport of an object by six pre-attached robots interacting via physical links. In *IEEE International Conference on Robotics and Automation (ICRA)*, pp. 1317–1323.

Lakshmikantham V and Trigiante D (1988) Theory of Difference Equations Numerical Methods and Applications. In *New York: Academic*.

Aitken VC and Schwartz HM (1994) On the exponential stability of discrete-time systems with applications in observer design. In *IEEE Transactions on Automatic Control*, vol. 39, no. 9, pp. 1959–1962.

Appendix

A. Proof of Lemma 3

Proof. In order to use the skew symmetric matrices, we first need to augment the force vector in (32) into 3D, as shown below,

$$\dot{\mathbf{F}}^{+} = \left(-L_a^{+} - \frac{M}{J} R_a^{+}(t)\right) \mathbf{F}^{+},$$

where $\mathbf{F}^{+} = (f_{1x}, f_{1y}, 0, f_{2x}, f_{2y}, 0, \cdots, f_{Nx}, f_{Ny}, 0)^T$ is a vector containing augmented 3D forces with 0 z-axis components. $L_a^{+} = (L_{ij}^{+})_{3N\times 3N}, \{i,j\} \in \{1,2,\cdots,N\}$, where

$$L_{ij}^{+} = \begin{cases} \begin{pmatrix} N-1 & 0 & 0 \\ 0 & N-1 & 0 \\ 0 & 0 & 0 \end{pmatrix} & \text{if } i = j \\ \begin{pmatrix} -1 & 0 & 0 \\ 0 & -1 & 0 \\ 0 & 0 & 0 \end{pmatrix} & \text{if } i \neq j \end{cases}$$

is an extended graph Laplacian matrix for the 3D case. $R_a^+(t) = \big(R_i^+(t)R_j^+(t)\big)_{3N\times 3N}$ is a collection of products of skew symmetric matrices, and

$$R_i^+(t) = \begin{pmatrix} 0 & 0 & r_{iy} \\ 0 & 0 & -r_{ix} \\ -r_{iy} & r_{ix} & 0 \end{pmatrix},$$

where r_{ix} and r_{iy} represent the subcomponent of $\mathbf{r}_i$ in the x and y axis, respectively. Note that $R_a^+(t)$ is time-varying since $\mathbf{r}_i$ changes while the object is rotating.

Notice that both L_a^+ and $R_a^+(t)$ are sparse because of the zero elements we introduced when lifting the 2D system to 3D in order to express the cross products as skew symmetric matrices. It will be helpful if we can eliminate the sparsity and only focus on the x and y dimensions. Consider every entry in the big $R_a^+(t)$ matrix,

$$R_i^+(t)R_j^+(t) = \begin{pmatrix} -r_{iy}r_{jy} & r_{iy}r_{jx} & 0 \\ r_{ix}r_{jy} & -r_{ix}r_{jx} & 0 \\ 0 & 0 & -r_{iy}r_{jy} - r_{ix}r_{jx} \end{pmatrix}. \tag{41}$$

Since $\mathbf{F}_j^+ = (f_{jx}, f_{jy}, 0)$, if we calculate $R_i^+(t)R_j^+(t)\mathbf{F}_j^+$, then the term $-r_{iy}r_{jy} - r_{ix}r_{jx}$ in (41) will be multiplied by zero and will disappear in the product. So we can eliminate the sparsity by removing the zero lines in $\mathbf{F}^+$, L_a^+ and removing the third column and third row in $R_i^+(t)R_j^+(t)$. The resultant matrix representation then matches what is shown in Lemma 3.

B. Proof of Proposition 2

Proof. Denote $\mathbf{r}_i$ using polar coordinates, $\mathbf{r}_i = (r_{ix}, r_{iy}) = (\|\mathbf{r}_i\|\cos(\theta+\theta_i), \|\mathbf{r}_i\|\sin(\theta+\theta_i))$, where θ is the angle of the object, which changes over time, and θ_i is the constant angle of $\mathbf{r}_i$ in the object's reference frame. Then we have

$$R_{ij}(t) = \|\mathbf{r}_i\|\|\mathbf{r}_j\| \begin{pmatrix} -\sin(\theta+\theta_i)\sin(\theta+\theta_j) & \sin(\theta+\theta_i)\cos(\theta+\theta_j) \\ \cos(\theta+\theta_i)\sin(\theta+\theta_j) & -\cos(\theta+\theta_i)\cos(\theta+\theta_j) \end{pmatrix}.$$

The first row of $R_a(t)$ is

$$\begin{aligned} R_a(1,:) = \|\mathbf{r}_1\|\sin(\theta+\theta_1)\Big(&-\|\mathbf{r}_1\|\sin(\theta+\theta_1), \\ &\|\mathbf{r}_1\|\cos(\theta+\theta_1), \cdots, -\|\mathbf{r}_N\|\sin(\theta+\theta_N), \\ &\|\mathbf{r}_N\|\cos(\theta+\theta_N)\Big). \end{aligned} \tag{42}$$

By observation, every row in $R_a(t)$ is linearly dependent on the first row because the $(2k-1)$-th and $(2k)$-th row, $k \in \{1, 2, \cdots, N\}$, of $R_a(t)$ can be written as

$$R_a(2k-1,:) = \frac{\|\mathbf{r}_k\|\sin(\theta+\theta_k)}{\|\mathbf{r}_1\|\sin(\theta+\theta_1)} R_a(1,:), \tag{43}$$

$$R_a(2k,:) = \frac{-\|\mathbf{r}_k\|\cos(\theta+\theta_k)}{\|\mathbf{r}_1\|\sin(\theta+\theta_1)} R_a(1,:). \tag{44}$$

Therefore, $rank\,(R_a(t)) = 1$ for any t.

Since the rank of $R_a(t)$ is one, it has only one nonzero eigenvalue. In order to find this eigenvalue, let us first look at its element, $R_{ij}(t)$. By solving $|\lambda I_{2\times 2} - R_{ij}(t)| = 0$ we can find the the eigenvalues and corresponding eigenvectors of $R_{ij}(t)$,

$$\begin{aligned} \lambda_1 = 0,\ \mathbf{v}_1 &= \big(\cos(\theta+\theta_j), \sin(\theta+\theta_j)\big)^T, \\ \lambda_2 &= -\|\mathbf{r}_i\|\|\mathbf{r}_j\|\cos(\theta_i - \theta_j), \\ \mathbf{v}_2 &= \big(-\sin(\theta+\theta_i), \cos(\theta+\theta_i)\big)^T. \end{aligned}$$

We can make several observations: the eigenvalues of $R_{ij}(t)$ remain constant regardless of the rotation of the object; the eigenvectors of $R_{ij}(t)$ rotate as the object rotates; $\mathbf{v}_1$ is a unit vector along $\mathbf{r}_j$; the direction of $\mathbf{v}_2$ can be acquired by rotating $\mathbf{r}_i$ clockwise by $\pi/2$ radians.

Denote $\mathbf{v}_2 = \big(-\sin(\theta+\theta_i), \cos(\theta+\theta_i)\big)^T$ as $\mathbf{e}_i$, which is the unit eigenvector associated with the non-zero eigenvalue of $R_{ij}(t)$. Then in general we have $R_{ij}(t)\mathbf{e}_i = -\|\mathbf{r}_i\|\|\mathbf{r}_j\|\cos(\theta_i - \theta_j)\mathbf{e}_i$, and $R_{ij}(t)\mathbf{r}_j = 0$. Also it is not hard to verify that $R_{ij}(t)\mathbf{e}_j = -\|\mathbf{r}_i\|\|\mathbf{r}_j\|\mathbf{e}_i$. Then we can construct a vector $\mathbf{e}_a = (\|\mathbf{r}_1\|\mathbf{e}_1, \|\mathbf{r}_2\|\mathbf{e}_2, \cdots, \|\mathbf{r}_N\|\mathbf{e}_N)^T$, which turns out to be the eigenvector of $R_a(t)$ because

$$\begin{aligned} R_a(t)\mathbf{e}_a &= \begin{pmatrix} R_{11} & R_{12} & \cdots & R_{1N} \\ R_{21} & R_{22} & \cdots & R_{2N} \\ \vdots & \vdots & \cdots & \vdots \\ R_{N1} & R_{N2} & \cdots & R_{NN} \end{pmatrix} \begin{pmatrix} \|\mathbf{r}_1\|\mathbf{e}_1 \\ \|\mathbf{r}_2\|\mathbf{e}_2 \\ \vdots \\ \|\mathbf{r}_N\|\mathbf{e}_N \end{pmatrix} \\ &= -\sum_{i=1}^N \|\mathbf{r}_i\|^2 \begin{pmatrix} \|\mathbf{r}_1\|\mathbf{e}_1 \\ \|\mathbf{r}_2\|\mathbf{e}_2 \\ \vdots \\ \|\mathbf{r}_N\|\mathbf{e}_N \end{pmatrix}. \end{aligned}$$

Hence, the only one nonzero eigenvalue of $R_a(t)$ is $\lambda_a = -\sum_{i=1}^N \|\mathbf{r}_i\|^2$, for any t. □

C. Analysis of Initial Random Trials

During the initial random trial phase, all the robots apply random forces to the object until their summed force is sufficient to break static friction. It is therefore important to estimate how many random trials need to be performed, especially when the number of robots is large, and each robot applies a small force.

Suppose that each robot randomly selects its own force $\mathbf{F}_i = (\frac{1}{N}f_{ix}, \frac{1}{N}f_{iy})$ such that f_{ix} and f_{iy} are both uniformly distributed on $[-f_{max}, f_{max}]$. When the number of robots N is large, and the force of each robot is correspondingly small, we know from the *Central Limit Theorem* that the summed force of all the robots is

approximately Gaussian distributed, that is

$$\sum_{i=1}^{N} \frac{1}{N} f_{ix} \approx \bar{f}_x \sim \mathcal{N}(\mu, \frac{\sigma^2}{N}),$$

$$\sum_{i=1}^{N} \frac{1}{N} f_{iy} \approx \bar{f}_y \sim \mathcal{N}(\mu, \frac{\sigma^2}{N}),$$

where $\mu = 0$ and $\sigma^2 = f_{max}^2/3$ are the mean and variance from the uniform distribution. We can further normalize $\bar{f}_x$ and $\bar{f}_y$ to the normal distribution, $\bar{f}'_x \sim \mathcal{N}(0,1)$ and $\bar{f}'_y \sim \mathcal{N}(0,1)$. Then the square sum $\bar{f}'^2 = \bar{f}'^2_x + \bar{f}'^2_y$ is distributed as according to the well-known Chi-squared distribution with degree 2, represented as

$$\bar{f}'^2 = \bar{f}'^2_x + \bar{f}'^2_y \sim \chi^2(2). \tag{45}$$

Given a friction $f_f < f_{max}$ that needs to be overcome by the robotic team, we can normalize it, denoted as $\bar{f}'_m$, as was done for $\bar{f}'_x$ and $\bar{f}'_y$,

$$\bar{f}'_m = \frac{\sqrt{N} f_f}{\sigma}.$$

Then we can find the probability of overcoming the friction in any one trial by looking up the Chi-squared distribution (45),

$$p_1 = \Pr(\bar{f}'^2 > \bar{f}'^2_m),$$

where the subscript 1 denotes the result of one trial. For the random process induced by successive independent trials (i.e. the Bernoulli process), it is well-known that the expected number of trials until the first success is $1/p_1$. Therefore, for any large (but finite) number of correspondingly weak robots, we expect to require a finite number of trials to break static friction (namely $1/p_1(N)$ trials, where $0 < p_1(N) < 1$). Unfortunately, $p_1(N)$ decreases with increasing N, hence it takes more trials to break static friction when there are more robots.